Joni Saastamoinen

Influence of the solute's molecular weight distribution on the spinnability of cellulose-ionic liquid solutions

School of Electrical Engineering

Thesis submitted in partial fulfillment of the requirements
for the degree of Master of Science in Technology Espoo, 6.9.2011

Supervisor: Professor Jukka Seppälä

Instructors: Ph.D. Michael Hummel
D.Sc. Sami Lipponen

Aalto-yliopisto
Teknillinen korkeakoulu

AALTO UNIVERSITY
SCHOOL OF ELECTRICAL ENGINEERING

ABSTRACT OF THE
MASTER'S THESIS

Author: Joni Saastamoinen

Title: **Influence of the solute's molecular weight distribution on the spinnability of cellulose-ionic liquid solutions**

Date: 6.9.2011 Language: English Number of pages: 7 +53

Department of Biotechnology and Chemical Technology

Professorship: Polymer Technology Code: Kem-100

Supervisor: Prof. Jukka Seppälä

Instructors: Ph.D. Michael Hummel, D.Sc. Sami Lipponen

The main experimental objective of this thesis was to investigate the effect of cellulose's weight distribution on the dry-jet wet spinnability and shear rheological properties of cellulose- 1-ethyl-3-methylimidazolium acetate (EMIMOAc) solution. Secondary object was to determine a relation between the spinnability and measured rheological properties of the spinnable solution.

The objective of the literature part was to review the field of spinning of polymer solutions and melts in order to acquire knowledge about the theoretical perspective of the experimental objective. This review contains general information and qualitative theories (presented theories offer qualitative value) about the spinning process which could be elaborated on in order to improve future investigations in this field (*e.g.* which questions need to be answered). Different authors who have pursued investigations and theories in the field of spinning have different views about this topic. Because of the lack of empirical results of cellulose-EMIMOAc solution spinning and universal theories about spinnability, quantitative expressions were not utilized in order to derive a connection between different steps of the experimental part. Derived relations were built on the order of magnitude of different parameters from MWD-, rheological and spinnability properties of the solutions which is rather qualitative approach to the main problem.

For the experimental task four cellulose-EMIMOAc solutions of varying molar mass distribution were prepared for spinning trials keeping weight average molar mass of the cellulose constant. The spinnability of each solution was investigated by determining the maximum draw-ratios which still enable stable spinning of the solution without filament break-up. Each solution was characterized by frequency sweep with a rotational rheometer. A relation between the maximum draw-ratio and increased polydispersity index (PDI) was observed after the spinning trials with three different solutions. Although it is difficult to define the optimal spinning conditions for different test solutions, it could be concluded that the spinnability of a cellulose-EMIMOAc solution increases due to increased proportion of high molecular weight cellulose chains.

Keywords: Ionic liquids, cellulose, dry-jet wet spinnability, rotational and elongational rheometry, Lyocell process

AALTO-YLIOPISTO
SÄHKÖTEKNIIKAN KORKEAKOULU

DIPLOMITYÖN
TIIVISTELMÄ

Tekijä: Joni Saastamoinen

Työn nimi: **Selluloosan moolimassajakauman vaikutus ioniseen nesteeseen liuotetun selluloosan märkäkehruuseen**

Päivämäärä: 6.9.2011 Kieli: Englanti Sivumäärä: 7 +53

Biotekniikan ja kemian tekniikan laitos

Professuuri: Polymeeriteknologia Koodi: Kem-100

Valvoja: Prof. Jukka Seppälä

Ohjaajat: TkT Michael Hummel, TkT Sami Lipponen

Tärkeimpänä päämääränä tässä työssä oli tutkia selluloosan moolimassajakauman vaikutusta selluloosa-EMIMOAc-liuoksen märkäkehruutyöstettävyyteen sekä leikkausreologisiin ominaisuuksiin. Toisena päämääränä oli tutkia yhteyttä kehrättävyyden ja mitattujen reologisten ominaisuuksien välillä. Märkäkehruu-menetelmä on analoginen Lyocell-prosessiin, jossa suuttimen ja vesialtaan välillä käytetään ilmarakoa.

Kirjallisuusosassa tarkoituksena oli tehdä katsaus polymeeriliuosten ja polymeerisulien kehruusta, jotta työn kokeelliselle osalle saataisiin teoreettista näkökulmaa. Katsaus sisältää yleistietoa sekä kvalitatiivisia teorioita (esitetyillä kaavoilla lähinnä kvalitatiivista arvoa) kehruu prosessista. Syventymällä esitettyyn tietoon ja teorioihin voidaan tulevaisuuden tutkimuksia saman aiheen ympärillä kehittää (esim. tutkimuskysymyksien asettelua voidaan tarkentaa). Tutkijat, jotka ovat esittäneet teorioitaan kehruunprosessiin liittyen, eivät jaa yhtenäistä näkemystä yksittäisten teorioiden paikkansapitävyydestä. Koska selluloosa-EMIMOAc-liuosten kehruusta ei ole kattavasti empiirisiä tuloksia eikä yleispäteviä teorioita kehruuseen liittyen löytynyt, kvantitatiivisia ilmauksia ei käytetty yhdistämään kokeellisen osan eri osa-alueita toisiinsa. Osa-alueiden välinen yhteys perusteltiin moolimassajakauma-, reologia- sekä kehrättävyysparametrien samaan suuruusjärjestykseen eri testiliuosten välillä.

Kolme erilaisen moolimassajakauman, mutta mahdollisimman saman lukukeskimääräisen moolimassan omaavaa selluloosa-EMIMOAc-liuosta valmistettiin koekehruita varten. Kunkin liuoksen kehrättävyyttä tutkittiin määrittämällä maksimi vetosuhde, jolla liuosfilamentteja voitiin vielä kehrätä häiriöttä ilman filamenttien katkeamista. Maksimi vetosuhteen ja kasvavan polydispersiteetti-indeksin välillä havaittiin olevan yhteys toisiinsa kolmen testiliuoksen kehruun perusteella. Vaikka erilaisten liuosten optimityöstöolosuhteiden määrittäminen on haasteellista, voidaan selluloosa-EMIMOAc-liuoksen kehrättävyyden päätellä paranevan korkean moolimassan selluloosaketjujen osuuden lisäyksen seurauksena.

Avainasanat: Ioniset nesteet, selluloosa, märkäkehräys, rotaatio- ja venymäreologia, Lyocell-prosessi

Acknowledgements

This thesis was carried out in the Department of Forest Products Technology of the Aalto University, School of Science and Technology within the Future Biorefinery (FuBio) research program. Thus thanks for the funding belong to Forestcluster and Tekes.

I wish to thank my instructors Michael Hummel and Sami Lipponen, Professor Herbert Sixta and Professor and supervisor Jukka Seppälä for their help and guidance during the writing of this thesis. I also wish to thank Alexandra Müller, Ronald Beyer, Denis Ingildeev and Frank Hermanuz from The Institute of Textile Chemistry and Chemical Fibers Denkendorf for their hospitality and support for the thesis. General thanks belong to all who have been supportive during this thesis project.

Contents

Experimental part:

Abbreviations

CL	cotton linters
DP	degree of polymerization
EMIMOAc	1-ethyl-3-methylimidazolium acetate
FS	frequency sweep
GPC	gel permeation chromatography
HDPE	high density polyethylene
IL	ionic liquid
LDPE	low density polyethylene
MWD	molecular weight distribution
NMMO	*N*-Methylmorpholine-*N*-oxide
PAN	polyacrylonitrile
PDI	polydispersity index
PP	polypropylene
PS	polystyrene

1 Introduction

Ionic liquids (ILs) such as 1-ethyl-3-methylimidazolium acetate (EMIMOAc) can be utilized as a direct solvent for cellulose. Cellulose fiber spinning from ionic liquids is comparable to spinning of cellulose-*N*-methylmorpholine *N*-oxide (NMMO) solutions which has been given the name 'Lyocell process'. The Lyocell process has been developed to offer economic, environmental and also fiber property improvements for fiber processing. The utilization of suitable ionic liquid instead of NMMO might develope these improvements even further. Addition of small fractions of high molecular weight cellulose has shown to be beneficial for the spinnability of the respective cellulose-NMMO solutions. In this thesis the same phenomenon is investigated with cellulose-EMIMOAc solutions.

The main objective of the experimental part was to determine if the MWD properties of the utilized solutions correlate with their respective maximum draw-ratios in the spinning trials. The secondary objective was to determine a relation between the shear rheological properties and maximum draw-ratios of the solutions. In order to fulfill these objectives following steps were included in the experimental execution: 1. molecular weight distribution (MWD) characterization of cotton linter blends utilized in the spinning solutions 2. rheological characterization of cellulose-EMIMOAc solutions 3. spinnability investigations which involved determining the maximum draw-ratio for different spinning solutions.

In the literature part the field of spinning rheology and polymer fluid spinnability was reviewed. The purpose of this review was to find ideas of how to relate the afomentioned steps of the experimental part in a theoretical level. Few authors [1, 2, 3] have given an extensive contribution to this theoretical aspect. Thus discussion about spinnability in this thesis is mainly based on their work. Presented observations from the spinning rheology and other related physical phenomena were found mostly from the work of Mortimer and Péguy [4, 5, 6]. Information from the literature part has been utilized as a tool for the analysis of the results in the experimental part. However, the most important value of this review is to serve as a starting point for the future development of spinnability investigations.

Any universal theory which would enable connecting the aforementioned experimental steps quantitatively was not found for the literature part. This situation follows from the complexity of the physical phenomena occurring in the spinning process. Thus precise mathematical modeling of the process is problematic. Theories which are universal are often impractical and simplified theories or empirically derived theories are often specific to the utilized system. Thus at the current state of this research field compromises between the universality and practicality of the mathematical tools for predicting spinnability of a polymer solution or melt has to be done.

2 Rheological characterization of spinning fluids

Theory presented here utilizes basic rheological parameters such as shear viscosity, rate, stress and moduli. These concepts are explained in several text books *e.g.* Mezger [7] explains these on a practical level. Text book from Ziabicki [1] gives a deeper insight to rheology applied to fiber spinning (melt, dry- and wet-spinning).

Based on the literature reviewed in this thesis, it seems to be essential to know the elongational rheological parameters of the spinning solution. The analogies between elongational parameters are the same as with shear rheological parameters. However, both measuring elongational rheology and deriving applicable relations between shear and elongational rheology is still a problem for scientists to overcome. The following discussion serves as an introduction to the statement of why shear rheological characterization is utilized in the experimental of this work.

All authors [1, 2, 3] referred to in chapter 5 present elongational rheology parameters in their mathematical models considering spinnability theories. Different methods utilized for this task include simplifications in the flow models and relations between shear and elongational parameters. However, these authors do not have a consensus of the optimal method to relate spinnability to rheological parameters or to measure elongational rheology. After a brief review of the methodology utilized in measuring elongational viscosity, Ziabicki [1] collects following conclusions about elongational flow (describing the level of knowledge about this field in 1976):

1. Steady-state elongational viscosity η^* (Trouton viscosity) at moderate deformation rates is nearly constant and equal to 3-times the Newtonian (zero shear) viscosity η_0 :

$$\eta^* \approx 3\eta_0$$

2. Steady elongational flow cannot be realized above some critical deformation rate where elastic deformation dominates viscous deformation;

3. Elongational flow of polymers is very sensitive to viscoelastic memory effects. For viscoelastic melts and concentrated solutions the memory effects in transient flow seem to be much more important than possible non-linear flow in steady-state conditions.

Recent development of the measurement techniques of elongational viscosity and relaxation times include: 1. Filament streching rheometer 2. Filament break-up rheometer. Shelley and McKinley [8] review briefly the development of both measurement methods. Despite this development, there is still no consensus of how to measure elongational viscosity.

In the experimental part of this work shear rheological parameters are connected to spinnability. Calculations of some shear rheological parameters presented in chapter 4.1 require the index *n* which can be acquired from the model of shear dependent viscosity referred as the Ostwald-de Waele power law [1, 9]:

$$\eta\left(\dot{\gamma}\right) = C\left|\dot{\gamma}\right|^{n-1} \tag{1}$$

where

η (Pas) is the viscosity

$\dot{\gamma}$ (1/s) is the shear rate

n is the power law index

C is constant

Even though rheology measurements in the experimental part of this thesis are executed by oscillation rheometry, this data should be applied to steady state shear. Cox-Merz rule relates complex viscosity η^* and apparent viscosity η_a:

$$\eta^*(\omega) = \eta_a\left(\dot{\gamma}_a\right) \tag{2}$$

where

ω (1/s) is the angular frequency which is equal to shear rate $\dot{\gamma}_a$ (1/s) for small-strain oscillatory motion

3 Dry-jet wet spinning & Lyocell Process

Dry-jet wet fiber spinning from direct cellulose solvents has so far been utilized in industrial scale with *N*-methylmorpholine-*N*-oxide-technology. This process has been given the name Lyocell process. Since dry-jet wet spinning from EMIMOAc solutions is novel and still lacks basic research of the whole process, thus the theories derived for NMMO-spinning serve as a benchmark for EMIMOAc-spinning. NMMO-technology is analogous to EMIMOAc-spinning while the solution structures differ from each other. Fink *et al.* [10] have reviewed the field of NMMO-technology. A schematic picture of the Lyocell process is presented in Figure 1.

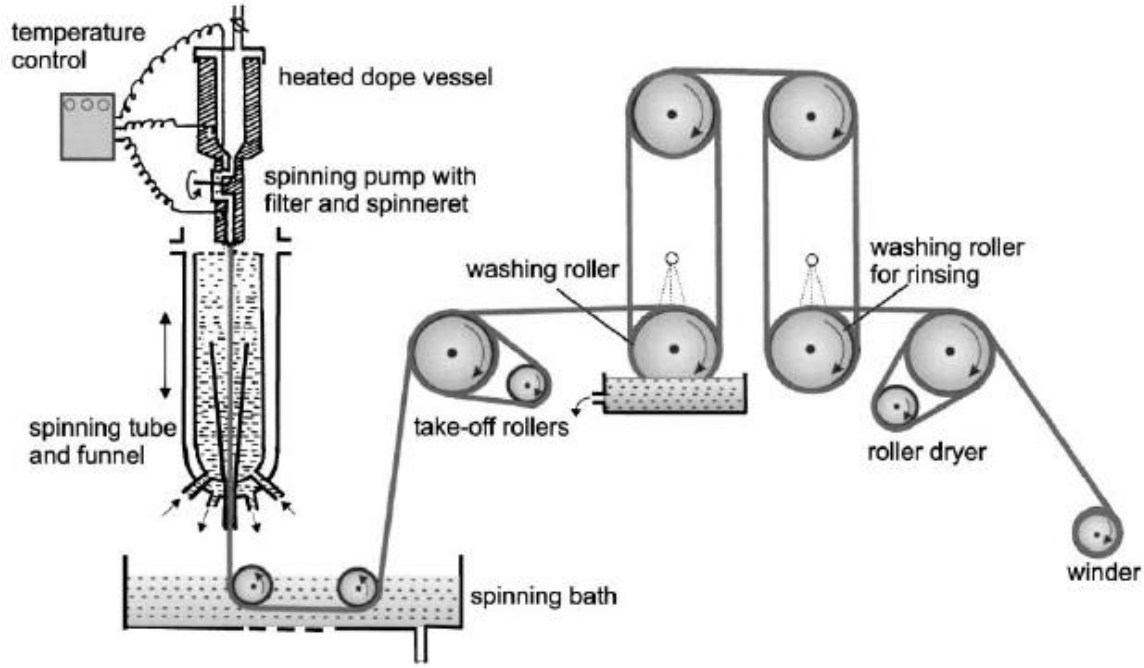

Figure 1. A schematic picture of the Lyocell process. [10]

Industrial fiber manufacture by NMMO technology contains at least following processing steps: [1, 10]

1. Preparation of the spinning dope by dissolution of the pulp in an NMMO-water mixture.
2. Extrusion of the spinning dope through an air gap into a precipitation bath.
3. Coagulation (solidification) of cellulose fibers in the precipitation bath.
4. Washing, drying and post-treatment (twisting, oiling, dyeing etc.).

Recovery of solvent is part of the industrial fiber processing. All the four processing steps influence final fiber structure and properties. Dry-jet wet spinning from EMIMOAc solution is analogous to NMMO-technology. Thus, aforementioned processing steps 1-4 could be stated similarly for the cellulose-EMIMOAc solutions. However, with EMIMOAc utilization of additional water may not be necessary.

There are many variations to execute fiber manufacturing but some operations are often similar in different methods. Thus some fundamental spinning parameters are also common for different spinning technologies. These technologies include widely utilized melt, dry- and wet-spinning from which the wet-spinning of cellulose derivatives (conventional viscose and cuprammonium solutions) is most similar to dry-jet wet spinning. The main difference to wet-spinning with dry-jet wet spinning is the use of an air gap where the polymers in the solution filaments can be oriented significantly. [10]

There is a common list of processing parameters which are influencing fiber formation in dry-jet wet spinning. Since these parameters are frequently utilized in the fiber spinning theory, they should be presented at this point:

Spinning temperature T (°C) referring to temperature of the solution when passing the spinneret

Volume flow Q (m^3/min) in the solution container that should equal volume flow in the spinneret

Extrusion velocity V_o (m/min) from the spinneret

Extrusion pressure P (Pa) in the solution container from which the pressure difference ΔP between the in- and outlet of the spinneret can be calculated.

Air gap length h (m)

Take-up (take-off) velocity V_L (m/min)

Coagulation bath temperature $T_{coagulation}$ (°C)

Equation of continuity can be applied to describe cylindrical form of the solution (or melt) filament in case of stable spinning. In the absence of mass transfer this equation can be presented in the form [1, p. 64]:

$$\rho R^2(x)V(x) = \rho Q = Const. \tag{3}$$

where

ρ (kg/m^3) is the density of the filament

$R(x)$ (m) is the radius of the filament at distance x

$V(x)$ (m/s) is the longitudinal velocity of the filament

Applying equation (3) for a single hole at the spinneret face, it is possible to calculate the extrusion velocity:

$$V_o = \frac{Q}{n_{jets} \cdot \pi \cdot r^2} \tag{4}$$

where

Q (m^3/min) is the volume flow of the extruded solution

n_{jets} is the number of holes in the spinneret

r (m) is the radius of one jet hole

Apparent draw-ratio (jet stretch/spin-draw-ratio) is a parameter indicating the relation between the take-up velocity and extrusion velocity:

$$Spin-draw\ ratio = \zeta_{app} = \frac{V_L}{V_o} \tag{5}$$

To emphasize the draw/stretching of the filament, a stretch ratio in percentages is utilized in the experimental part of this thesis:

$$Jet\ stretch\ \ ratio\,(\%) = \frac{V_L - V_o}{V_o} \cdot 100\,\% \tag{6}$$

4 Solution rheology in the spinning process

The following sub-chapters cover some theories about rheology in spinning which are either experimentally verified or have a simple form. The field of rheology in spinning is also covered in a more mathematical and fundamental level by several authors [1, 11, 12]. From these authors, Ziabicki [1] presents qualitative and simple form equations (as well as more complex ones) and empirical observations about fiber spinning (which is needed to verify theories).

The field of structure formation in polymer melt and solution spinning is a widely investigated. Several authors have investigated structure formation of Lyocell fibers. This topic is reviewed by Fink *et al.* [10]**.** Examples of authors who have investigated the effect of physical processing parameters on the structure formation include: Mortimer *et al.* [4, 5, 6 (*e.g.* draw-ratio, air gap length) and Weigel *et al.* [13] (length to diameter ratio of the spinneret nozzle). The effect of physical processing parameters on the solution rheology will be discussed in the following subchapters.

Publications about investigation on the structure properties of fibers spun from ionic liquids are also available: *e.g.* Wendler *et al.* [14] and Kosan *et al.* [15] have spun cellulose fibers from different ionic liquids and compared resulting fiber properties to each other and to NMMO-fibers. However, these investigations do not cover a systematic relation between physical processing parameters and resulting structure and mechanical properties of the fibers.

4.1 Structure formation in the spinneret

Flow behavior of the solution in the spinneret and air gap is mathematically complex and thus only some ideal condition equations for shear rates and stresses are presented here. For a shear thinning fluid in an infinitely long capillary the so called ‘power law’ can be utilized to calculate shear rate (velocity gradient) $\dot{\gamma}$ on the capillary wall and viscosity in the capillary as shown by equations 7-9. Parameter *n* is 1 for a Newtonian fluid. [1, pp. 51 and 261]

$$\dot{\gamma} = \left(\frac{\delta V_x}{\delta r} \right)|_{r=R_0} = -\frac{3n+1}{n} Q/(\pi R_o^{(n+2)/n}) = -\left(\frac{\Delta P R_0}{2\eta l_0} \right) \tag{7}$$

where

Q (m^3/s) is the volumetric velocity of the solution.

R_0 (m) is the radius of the capillary

n is the power law index of the solution

l_0 (m) is the length of the capillary

ΔP (Pa) is the pressure difference between the inlet and outlet of the capillary

η (Pas) is the viscosity of the solution in the capillary

V_x (m/s) is the velocity in the direction of flow at filament radius r (distance from the cylinder axis)

$$Q = \frac{n}{3n+1}\pi R_0 \left(\Delta P R_0^3 / 2\eta l_0\right)^{1/n} \tag{8}$$

Viscosity can be extracted from the equation (9):

$$\eta = \frac{\Delta P R_0^3}{2l_0\left(\frac{Q(3+1/n)}{\pi R_0}\right)^n} \tag{9}$$

Michels and Kosan [16] and Collier *et al.* [17] have considered the deformation in the spinneret to be dominated by elongational rather than shear influence. The former [16] present a mathematical model for the elongational deformation in the spinneret and air gap (Presented in Figure 2 with schematic picture of the spinneret and air gap). Elongation deformation rate in the spinneret is given by equation (10):

$$\dot{\varepsilon}_D = \frac{\Delta P}{\eta_D} = \frac{v_e}{l_0} e^{\ln\left(\frac{D_E}{D_A}\right)^2 - 1} \tag{10}$$

where

ΔP (Pa) is the pressure difference between the in- and outlet of the spinneret

η_D (Pas) is the elongational viscosity of the solution

v_e (m/s) is the velocity of the solution at the inlet of the spinneret

l_0 (m) is the length of the spinneret channel

D_E (m) is the diameter of the inlet hole

D_A (m) is the diameter of the outlet hole

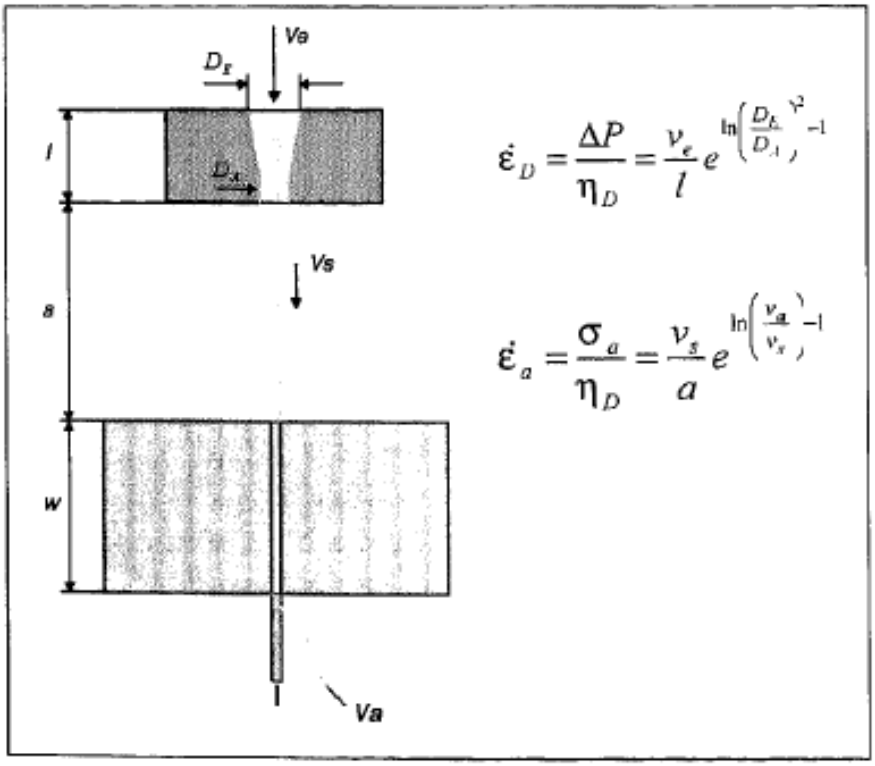

Figure 2. Elongation deformation in the die (spinneret) channel and air gap. [16]

4.2 Die swell

Elastic nature of polymer solutions and melts causes swelling of the fluid filament when it is extruded from the spinneret. The degree of this swelling can be measured with die swell ratio χ: [1, p. 57]

$$\chi = \frac{R_{\max}}{R_0} \tag{11}$$

where

R_{max} (m) is the maximum radius of the filament

R_0 (m) is the radius of the capillary (spinneret)

Die swell can also be written in the form of equation (12) when there is negligible amount of mass transfer from or to the filament: [1, p. 261]

$$\chi = \left(\frac{V_0}{V_f}\right)^{1/2} \tag{12}$$

where

V_f (m/s) is the velocity of the filament with the maximum radius R_{max}

V_0 (m/s) is the velocity of the filament at the spinneret face

Die swell is dependent on shear rate $\dot{\gamma}$ and the relation between residence time t^* and relaxation time τ: [1]

$$\chi = \chi\left(\dot{\gamma}, t^* / \tau\right) \tag{13}$$

The time for the solution to pass a capillary of length l_0 is called residence time: [1]

$$t^* = \pi R_0^2 l_0 / Q \tag{14}$$

Die swell (extrudate swell) defines the shape of a filament at the spinneret face and thus the following filament rheology and dynamics are dependent on it. More quantitative descriptions for die swell can be found for instance from Ziabicki [1, pp. 57-61] and Chapoy [18] who describes swelling as a result of two separate parameter groups: 1. dynamics of the flow in the capillary and 2. the memory of the fluid. White and Roman [19] have investigated the relation between die swell, rheological properties and take-up force in melt spinning.

Equations (7)-(9) describe steady-state flow which can theoretically occur only in infinite capillaries for viscoelastic fluids. Ziabicki [1, pp.51-55] presents the relation between residence and relaxation time as the critical factor for steady-state assumptions. To reach steady flow, longer residence times than relaxations times would be required. Interestingly, White and Ide [20] claim that the deformation rate dependence on relaxation time is important in modeling filament break-up in melt-spinning (which is considered in chapter 5). Thus setting boundaries for the applicability of 'power law' in describing fiber spinning might be complex.

4.3 Structure formation in the air gap

Mortimer *et al.* [4, 5, 6] have investigated the filament formation, thermodynamics, rheology (which are all related to each other) and also the overall fiber structure formation in the air gap and coagulation bath by observing the diameter, birefringence and temperature profiles of deformed filaments and solidificated fibers during the spinning process. Michels and Kosan [16] and Collier *et al.* [17] have presented mathematical equations concerning elongational rheology in the spinneret air gap. Liu *et al.* [21] have examined Lyocell process as a melt-spinning process from the air gap part. Since Mortimer *et al.* [4, 5, 6] have presented empirical observations from NMMO dry-jet wet spinning, it is mainly their work which is presented here.

4.3.1 Filament temperature and shear viscosity

By measuring the temperature of the filament in the air gap as a function of the distance from the spinneret, Mortimer and Péguy [4] observed an exponential relation between the two variables. Experiments were executed with the air gap length of 250 mm and spinneret (monofilament) diameter of 500 µm. The authors [4] observed that a function of the form of equation (15) fits well with the experimental values. Ziabicki [1, pp. 78-81] has presented a theoretical model for the filament thermodynamics which leads to a

similar filament surface temperature versus the distance from the spinneret relation as in equation (15):

$$\frac{T(x)-T_{\infty}}{T_0-T_{\infty}}=e^{-ax} \tag{15}$$

where

T_{∞} (K) is the ambient temperature

T_o (K) is the temperature of the spinneret

a is arbitrary constant that takes into account different effects such as evaporation and viscous flow

x (m) is the distance from the spinneret

Equation (15) states that the surface temperature of a filament decreases exponentially with distance from the spinneret. Many empirically derived equations state that polymer melt or solution viscosity increases exponentially as a function of decreasing temperature [1, pp. 30-31]. This observation together with the relation indicated by equation (15) has led authors [4] to the assumption that the shear viscosity of a solution filament increases exponentially with increasing distance from the spinneret face. This assumption was tested by comparing experimental data relating (solution) viscosity to temperature from Navard *et al.* [22] and data relating temperature to distance from the spinneret (from the authors [4]). Assumption seemed to hold true for viscosity data which was measured from diluted solutions. Authors [4] claimed to test the hypothesis with data gained from concentrated solutions. However, the lack of data points prevented derivation of a mathematical model for the relation.

Authors [4] noticed that the filament's surface temperature after the air gap of 250 mm is approximately the same as the ambient temperature. Thus the effect of thermal quench in the coagulation bath is negligible. With reducing air gap length this effect was expected to increase.

4.3.2 Filament velocity and elongational viscosity

Filament shape formation in the air gap has been investigated in terms of dimensionless velocity V/V_0. Dimensionless velocity can be related to filament diameter by applying equation (16):

$$\frac{V}{V_0}=\frac{d_0^2}{d^2} \tag{16}$$

where

V (m/s) is the velocity of the filament part having the diameter d

V_0 (m/s) is the velocity of the filament part having the diameter d_0 at the spinneret face

Authors [4] monitored dimensionless velocity as a function of the distance from the spinneret and compared these results to the theoretical function of the same relation. The dimensionless velocity was calculated from the observed filament diameter with the equation (16). Experiments were executed with two different monofilament spinneret diameters 200 and 300 µm using the same draw-ratio with both spinnerets. Theoretical function was concluded starting from the equation (17) with the assumptions of zero relaxation after the spinneret flow (no die swell), zero air drag, constant extensional force and the aforementioned exponential behavior for elongational viscosity in the air gap. Following these assumptions, spinning was modeled as uniaxial flow. The assumption of a constant extensional force has been predicted by Denn and Petrie [23]. This assumption should hold true for low stresses. Extensional stress $\tau_{elongation}$ can be written:

$$\tau_{elongation} = \dot{\varepsilon}\,\eta_E \tag{17}$$

where

$\dot{\varepsilon}$ (1/s) is the extension rate

η_E (Pas) is the extensional viscosity

Equation (17) can be written in the form:

$$\frac{F}{A} = \eta_E \frac{dV}{dx} \tag{18}$$

where

F (N) is the extensional force

A (m^2) is the cross-sectional area of the filament

V (m/s) is the thread line velocity

x (m) is the distance from the spinneret

Equation (18) can be further transformed to a form:

$$\frac{d\,\ln V}{dx} = \frac{1}{\eta_e}\frac{F}{Q} \tag{19}$$

where

$Q = VA$ (m^3/s) is the volumetric flow of the filament

With the aforementioned assumptions, equation (19) was transformed to equation (20) by the authors [4]:

$$\frac{V}{V_0} = D_R \exp[-\ln D_R \exp(-ax)] \tag{20}$$

where

a is a constant which takes into account effects such as mass transfer viscous flow.

D_R is $\frac{V}{V_0}$ for x $\rightarrow \infty$

Theoretically and experimentally gained dimensionless velocity versus distance from the spinneret data are compared in Figure 3. As can be seen from the picture, the experimental results follow well theoretical model. Assuming appropriate measurement data, equations (16)-(20) give a possibility to evaluate filament form, velocity, elongational tension and viscosity in the air gap. [4]

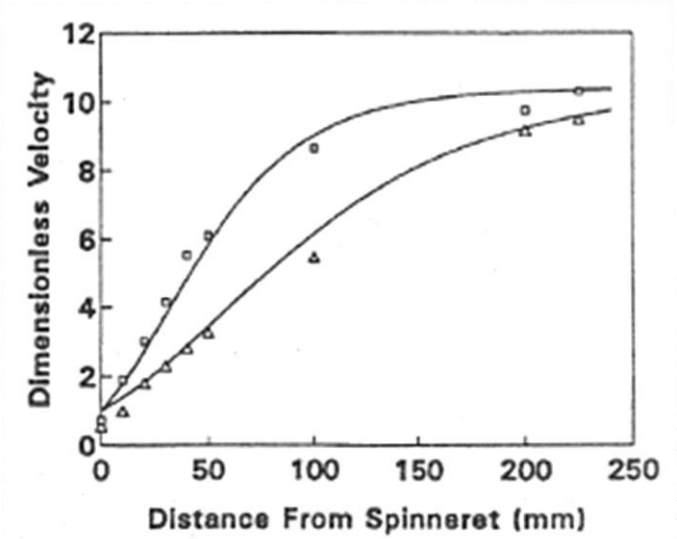

Figure 3. Dimensionless velocity of the filament as a function of distance from the spinneret: (□) 200 μm, (triangle) 300 μm spinneret, (-) fitted curve. [4]

Both curves in Figure 3 increase to almost same final value but with a 300 μm spinneret this happens slower. Authors [4] claim that the slower velocity increase of the thicker filament follows from the differences in specific surface area which is related to the efficiency of the cooling of the filaments. This theory is presented in a mathematical form by Ziabicki [1, p. 81]. Authors also observed die swell effect to be smaller for the thinner filament. This is related to aforementioned faster cooling and viscosity increase of the thinner filament. [4]

Uniaxial, steady-state, isothermal Maxwell liquid model for the filament velocity V (which is an average value of the velocity distribution) can be written as a function of the distance from the spinneret: [1, pp. 64-68]:

$$\begin{aligned} &3\eta_0 \ln(V/V_0) + C\tau(V - V_0) = Cx \\ &C = 3\eta_0 \ln(V_L/V_0)\left[L - \tau(V_L - V_0)\right]^{-1} \end{aligned} \tag{21}$$

where

L (m) is the length of the filament

V_L (m/s) is the velocity at the end of the filament

It can be seen that equation (20) gives dimensionless velocity V/V_0 explicitly while equation (21) is an implicit function of V/V_0 and x. Thus, it is not possible to extract only V/V_0 to the left side in equation (21). Equation (21) is more complicated of the two despite the fact that it is supposed to describe simpler filament flow. Both equations require experimental data of the filament velocity with the specific spinning parameter setting. Also equation (21) utilizes rheological parameters of the solution. The problem of losing the generality by deriving equations empirically and losing practicality by deriving them theoretically is faced in every aspect of quantitative description of the spinning process.

Michels and Kosan [16] present equation (22) for calculating elongation rate $\dot{\varepsilon}_a$ in the air gap:

$$\dot{\varepsilon}_a = \frac{v_s}{a} \cdot e^{\ln\left(\frac{v_a}{v_s}\right)-1} \tag{22}$$

where

v_s (m/s) is the injection (extrusion) velocity

v_a (m/s) is the take-up velocity

a (m) is the air gap length

As can be seen, equation (22) expects the elongational rate to be constant in the air gap. Mortimer *et al.* [4] derived some theories considering the extensional viscosity and stress, but mathematical interpretations for these were described rather qualitatively. Thus it is not possible to evaluate, whether elongation rate calculated from the viscosity and stress would be equal to equation (22).

4.3.3 Air gap length and filament draw length

Mortimer and Péguy [5] concluded that a solution filament has a draw length, $D_{L,}$ which is the distance from the spinneret where the filament is fully drawn and where the diameter and velocity have reached their final values. At the draw length the filament is too cold and thus too viscous to be drawn any further. [5]

The aforementioned draw length of a solution filament was predicted theoretically and verified experimentally by the authors [5]. Theoretical aspect was based on the temperature change of the filament in the air gap. This model suggested that cooling of a filament depends only on the spinneret diameter, volumetric velocity, the distance from the spinneret and average diffusion rate for the temperature change on the filament surface. None of these parameters was considered to be dependent on the velocity of the filament. Thus authors [5] came to a conclusion, that the draw length is independent of the utilized draw-ratio. Empirical verification for the theory was executed by presenting measured values of the scaled diameter of the filament as a function of the distance from the spinneret. These results showed (presented in Figure 4) that with a fixed spinneret diameter and volumetric velocity but varying draw-ratio the recorded scaled diameters followed the same curve as a function of the distance from the spinneret. Decreasing volumetric velocity and spinneret diameter caused the decrease of the scaled diameter values and draw length. Scaled diameter ξ is calculated with the equation (23):

$$\xi = \frac{\varphi(z) - \varphi_f}{\varphi_0 - \varphi_f} \tag{23}$$

where

$\varphi(z)$ is the diameter at distance z

φ_0 is the initial diameter

φ_f is the final diameter

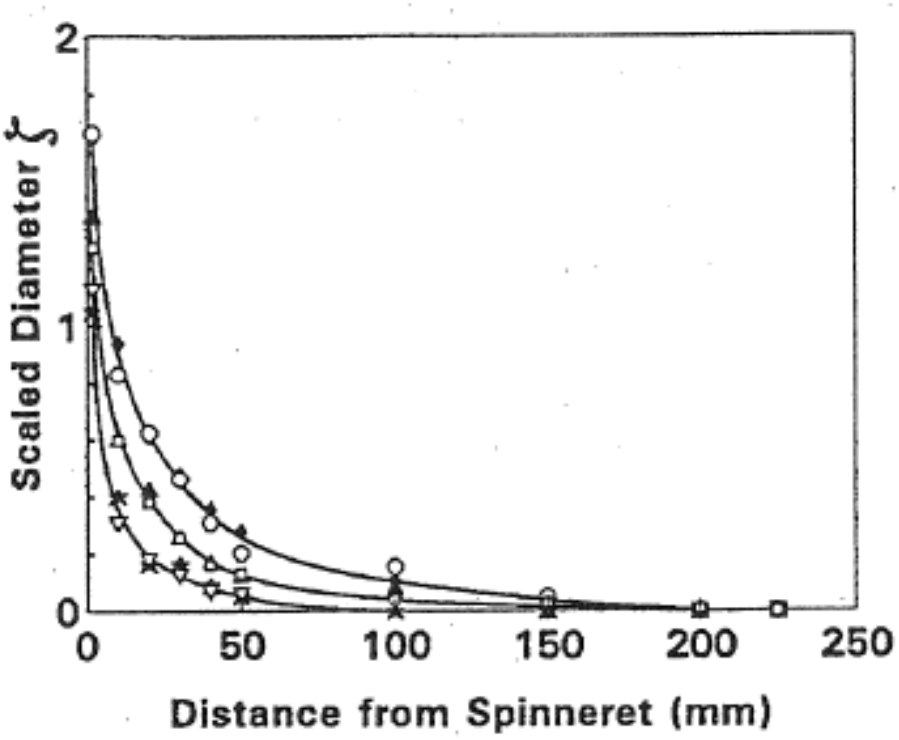

200 μm spinneret, Q = 1.2 mm³/s: □ D_R = 10.4; ▲ D_R = 15.4.
200 μm spinneret, Q = 1.6 mm³/s: ○ D_R = 7.8; ◆ D_R = 10.4.
150 μm spinneret, Q = 0.68 mm³/s: ★ D_R = 3.6; ▽ D_R = 10.4.

Figure 4. Measured scaled diameter ξ as a function of distance from the spinneret with different volumetric velocities Q and draw-ratios (D_R). Symbols are explained below the diagram. [5]

Mortimer and Péguy [6] examined the effect of varying air gap length on filament diameter and velocity profiles. It was noticed that adjusting the air gap length smaller than the draw length while keeping other parameters fixed had a great influence on the diameter profiles of the spun filaments. This phenomenon was considered to follow from the insufficient time for a filament to stabilize. The same explanation was utilized for the reduction of die swell following the decrease of the air gap length especially with short air gaps (disappeared completely with 10 mm air gap). With the air gap of 10 mm authors observed draw resonance phenomenon. Draw resonance has earlier been

reported widely to occur in melt spinning (will be discussed in Chapter 5.) Same phenomenon has also been observed in cellulose-NMMO- spinning [24].

4.3.4 Filament birefringence and tension

The most common method for investigating fiber structure formation of a running solution filament-solidificated fiber is birefringence measurement. When used as an on-line technique, it offers the possibility to examine the structure development of the fiber in different phases (spinneret, air gap, coagulation bath) of the spinning process. [1, pp. 202-204] Mortimer and Péguy [25] have utilized birefringence measurement for observing orientation development in dry-jet wet spinning. Authors [4] also related birefringence to tension affecting on the filament.

In order to derive this relation, birefringence on-line from the filament-fiber system was measured as a function of the distance from the spinneret [4]. These results are shown in Figure 5. When Figure 3 and Figure 5 are compared, it can be seen that their shapes are similar. Thus this has led to the assumption that there is a linear relationship between the dimensionless velocity and birefringence. This relation is shown in Figure 6. As was stated before, extensional force is expected to be almost constant in the air gap. Thus stress affecting the filament in the air gap should be proportional to the cross-sectional area of the filament which on the other hand is related to dimensionless velocity as shown by equation (16). From these relations it was concluded that birefringence is linearly proportional to stress on the filament. [4] However, later an exception to this behavior was observed when the draw-ratio was high enough to cause chain slippage [5]. Assumed chain slippage was observed for a 100 µm filament with draw-ratio of 10.4 and 200 µm filament with draw-ratio of 15.4. The reason for chain slippage to occur more easily for the thinner filaments was thought to result from the more efficient cooling of thinner filaments. [4, 5]

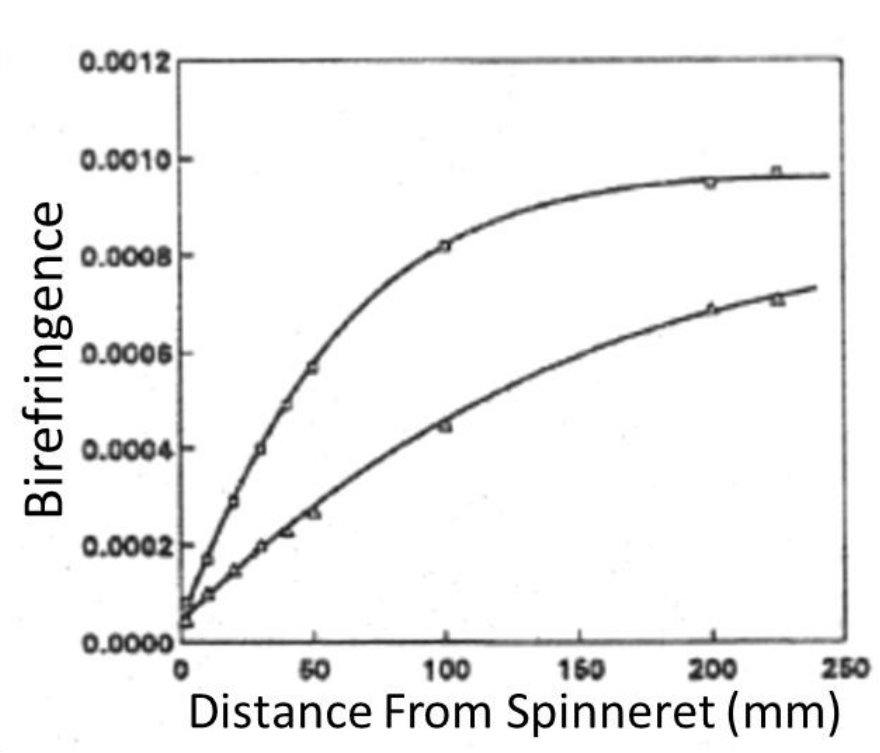

Figure 5. Birefringence of the filament as a function of distance from the spinneret: (□) 200 μm, (triangle) 300 μm spinneret, (-) fitted curve. [4]

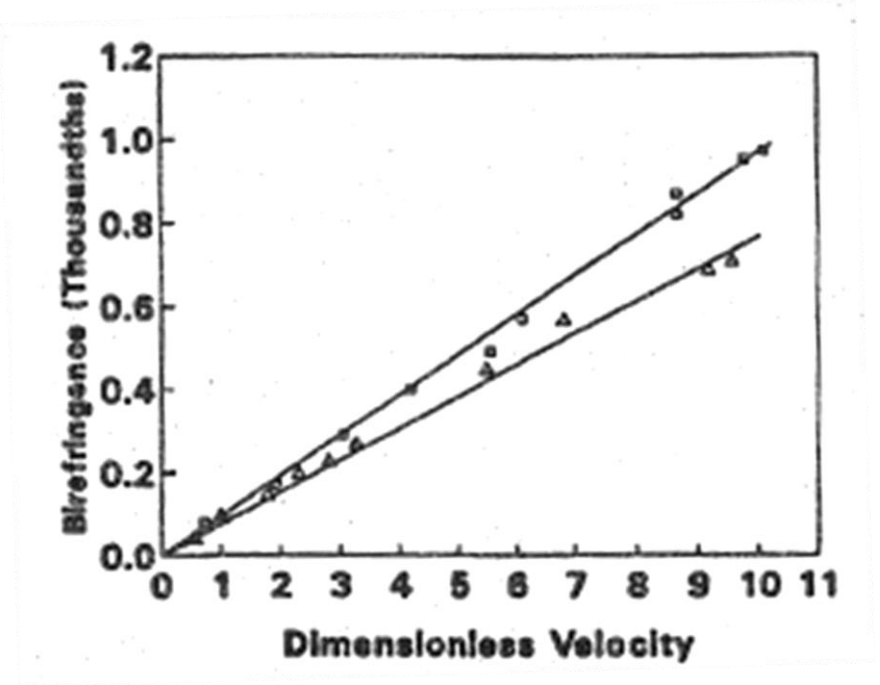

Figure 6. Birefringence of the filament as a function of dimensionless velocity (□) 200 μm, (triangle) 300 μm spinneret, (-) fitted curve. [4]

5 Spinnability of a polymer dope

5.1 Definition of spinnability

The term spinnability has no precise definition in fiber technology. Examples of definitions for spinnability are ‘the ability of making fibers from a given set of materials’ by Paul [26], ‘the ability to form threads’ by Ide and White [2] and Ziabicki [1] refers to spinnability as ‘the maximum attainable elongation’. All authors [1, 2, 3] seem to relate the quantitative description of spinnability to non-stable spinning which is introduced in the chapter 5.1.

From the practical point of view when only processing parameters are monitored, spinnability limits can be related to parameter limits which allow stable spinning. For this thesis, the draw-ratio was chosen for this purpose. Monitoring only the maximum take-up velocity (Tan. *et al.* [27] for PAN precursor fiber dry-jet wet spinning) would require keeping the extrusion velocity on the same level if any comparison between different spinning solutions would be executed (and was, hence, applied in this thesis).
Draw-ratio has a strong effect on the diameter profile and thus the maximum attainable elongation of the spun filament as was visible with the investigations carried out by Mortimer *et al.* [5] From this qualitative notification it could be stated that the maximum draw-ratio correlates with the maximum elongation. Thus the mentioned experiment might be suitable for determining spinnability as defined by Ziabicki [1]. Especially earlier spinnability investigations were executed by pulling polymer fluid threads with a rod and observing maximum attainable draw lengths and draw velocities. This type of investigation method has been utilized by Hashimoto and Imae [28] for aqueous polymer solutions.

The effect of spinning conditions on the fiber quality could also serve as a spinnability condition. However, the structure of a solidificated fiber depends strongly on the coagulation phase which is not as dependent on the rheological phenomena. Birefringence and thus orientation of the fiber is increased with draw ratio to some extent as was shown by Mortimer and Péguy [4]. Thus maximum attainable orientation might be a possibility for relating fiber quality to spinnability. Still it is not evident that all the mechanical properties of fibers are improved with the increased maximum elongation/draw. Thus the spinnability definitions utilized in the experimental of this thesis are not necessarily limits for the structure formation.

5.2 Non-stable spinning

Spinnability is usually limited by the break-up or instability of the filament forming. In order to gain quantitative expressions for the spinnability limits, the physical mechanism behind them should be understood. One requirement which covers all the introduced phenomena which limit spinnability is the time independence of various physical variables related to continuous spinning. These variables (indicated here by ξ) include all the kinematic, thermodynamic, dynamic and structural coefficients. In a mathematical form this independence can be stated: [1]

$$\frac{\partial \xi(x)}{\partial t} = 0 \tag{24}$$

Filament break-up and draw resonance are practically observed instabilities affecting fiber spinning generally (melt spinning, dry- and wet spinning) and especially polymer solution spinning. Filament break-up can happen via various mechanisms. At least three break-up methods occurring in fiber spinning have been introduced qualitatively: 1. Capillary break-up 2. Ductile-failure 3. Cohesive, brittle fracture. Ziabicki [1] reports only cohesive and capillary break-up methods while White and Ide [2, 29] add ductile failure to this list. These break-up methods are presented schematically in Figure 7.

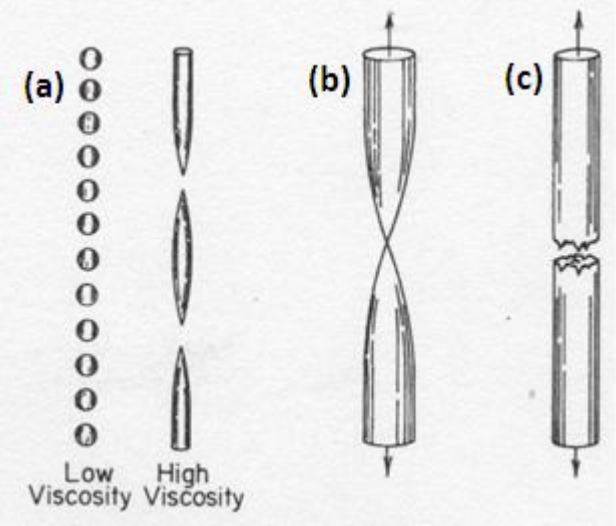

Figure 7. Mechanisms of filament instability/break-up: (a) capillarity; (b) ductile failure; (c) cohesive fracture. [2]

These aforementioned break-up mechanisms are introduced in the following chapters. Also draw-resonance and other instabilities which do not necessarily involve any filament break-up are described qualitatively. This information is based mainly on descriptions from Ziabicki [1] and White and Ide [2, 32]. Along these examples more recent studies are shown in order to introduce the computational development of break-up modeling. From the reviewed literature about break-up mechanisms it can be concluded that 1. There is no consensus about the physical nature of different break-up mechanisms. 2. In practice a combination of different break-up mechanisms may occur [3, 30].

5.2.1 Cohesive, brittle failure

Several authors [1, 2, 3] accept cohesive fracture as one of the break-up mechanisms. To some extent same authors seem to agree with Ziabicki's qualitative description of cohesive failure mechanism to follow from excessive storage of elastic energy. Recent investigation field considering brittle like failure includes microscopic aspect of the phenomenon [31].

Ziabicki [1, p. 27] claims that in technical practice cohesive failure determines the upper limit of take-up velocity and draw-ratio. Further, theoretical work suggests that relaxation time, tensile strength of the material and deformation conditions control

cohesive mechanism. For a linear viscoelastic fluid (Maxwell fluid) this type of break-up will occur once a critical stress level p^*, expressed by equation (25) is reached: [1, p. 15]

$$p^* = \sqrt{2KE} \tag{25}$$

where

K (J/m^3) is the critical elastic energy per unit volume

E (Pa) is Young's modulus

Elongational rate of the filament is supposed to be above a critical value in order to reach the breaking level: [1]

$$\dot{e}_{xx} \geq \left(2K / E\tau^2\right)^{1/2} \tag{26}$$

where

τ (s) is relaxation time

If tensile strength $p^*$and filament tension p_{xx} are modeled as a function of the distance from the spinneret, following condition should be reached at the fracture point, x^*_{coh}: [1]

$$p^*(x)|_{x=x^*} = p_{xx}(x)|_{x=x^*} \tag{27}$$

Figure 8 presents schematically the development of cohesive strength and filament tension up to the fracture point.

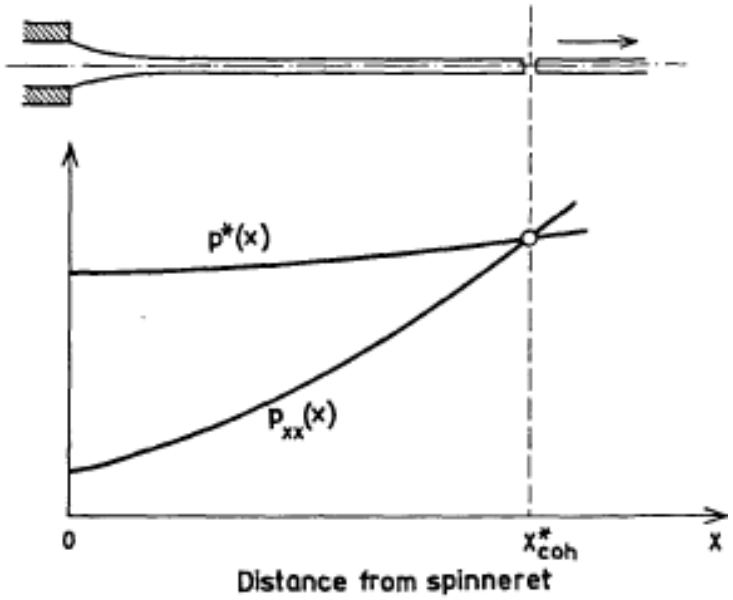

Figure 8. Cohesive fracture of a steady state liquid jet. [1, p. 16]

Han [3] has presented tensile stress as the limiting factor for solution spinnability in case of cohesive fracture although he has chosen a different physical model for the fracture mechanism than Ziabicki [1] has. White and Ide [2] have made an assumption

that with some critical stress cohesive fracture might be the break-up mechanism for all viscoelastic materials.

As an example of cohesive break-up occurring in practice, Ziabicki mentions that cohesive failure has been observed at least in melt spinning of high-molecular-weight polyolefins and in dry- and semi-melt-spinning of some solutions. Based on experiments with wet-spinning of acrylic fibers, Paul [26] has come to a conclusion that cohesive fracture is the main mechanism occurring in wet spinning. White and Ide [32] report low density polyethylene (LDPE) and polystyrene (PS) to fail by cohesive failure in melt spinning (PS only at high elongational rates).

5.2.2 Ductile failure

White and Ide [2] refer to ductile failure as a 100 % reduction in the cross section of the filament following from a high local stress level. Authors considered this break-up mechanism to be analogous to failure of solid metals and polymers. This kind of break-up mechanism was observed in melt spinning of high density polyethylene (HDPE) and polypropylene (PP) [29, 32]. Polystyrene (PS) was observed to show ductile failure with low and cohesive with high elongational rates [32]. Hassager *at al*. [30] have executed theoretical simulations to model ductile failure of Newtonian and viscoelastic fluids. They concluded that surface tension will affect ductile failure. Hassager *et al.* [30] mentions that ductile failure is combined with capillarity in practice. On the other hand, White and Ide [2, 20] mention the possibility of combinations of all three mechanisms. Some authors [33, 34] present ductile and cohesive, brittle like break-up mechanisms are thought to be the only ones to be expected with viscoelastic liquids. Malkin and Petrie [33] have reviewed the topic of cohesive and ductile break-up and given some critical evaluations on this classification as well as the physical nature of elastic and brittle-like failure (utilizing the word rupture). Wang *et al.* [34] have solved this classification problem by utilizing the word elastic break-up for ductile and brittle failure.

5.2.3 Capillary break-up

Capillary break-up is widely understood as a surface tension-induced break-up of filaments into drops or ligaments. Mathematical models of the break-up of Newtonian and non-Newtonian liquids often intersect. This is because the theories for the non-Newtonian viscoelastic liquids are often treated with assumptions of Newtonian behavior. Eggers [35] has reviewed the theoretical aspect of this kind of break-up for Newtonian fluids with a brief insight to such theory for viscoelastic fluids. This review covers linear and non-linear analysis of the surface tension flows.

Ziabicki [1, pp. 17-25] explains capillary break-up to follow from ‘capillary waves’ on the free surface of a liquid filament. Capillary waves are axisymmetrical disortions of the filament surface δ_0 which grow spontaneously leading to the break-up of the filament into drops. Ziabicki claims that in general the capillary instability determines the lower limit of the extrusion velocity and spinneret radius. Equation (28) gives a mathematical description for the capillary waves as a function of time *t* and the distance from the spinneret *x*:

$$\delta(t) = \delta_0 \exp(\mu t)\cos(2\pi x/\lambda); \lambda > 2\pi R \tag{28}$$

where

R (m) is the undistorted filament radius

λ (m) is the wavelength

μ is the growth factor

$\delta(t)$ (m) is the magnitude of the capillary wave

Capillary break-up should occur when the growing amplitude of capillary waves reaches the undistorted radius, R(x), of the filament. A general condition for the capillary break-up of the filament is of the form: [1]

$$\delta(x)|_{x=x^*} = R(x)|_{x=x^*} \tag{29}$$

where

x^* (m) is the distance from the spinneret where the break-up occurs

Figure 9 presents the development of capillary waves and radius of the filament as a function of the distance from the spinneret. The break-up point is at x^*_{cap}.

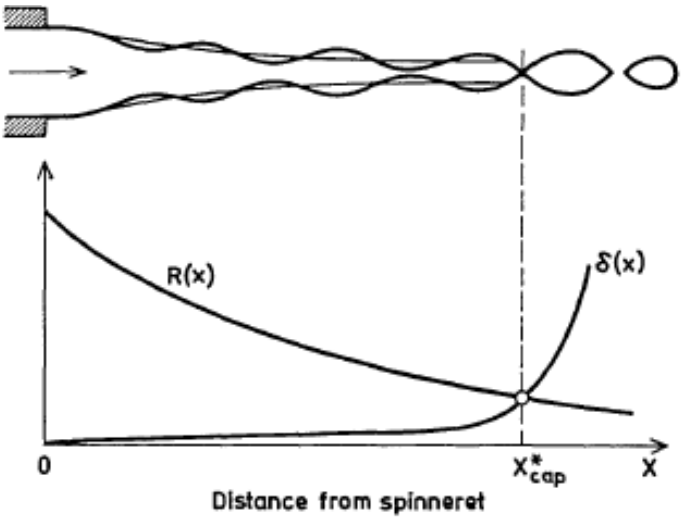

Figure 9. Break-up of a liquid jet due to capillary wave mechanism. [1, p. 18]

Weber [36] has derived an equation for the most probable (optimum) growth factor, μ_{opt}:

$$\mu_{opt} = (\alpha/R_0)/\left[6\eta + (8\rho\alpha R_0)^{1/2}\right] \tag{30}$$

where

α (N/m) is the surface tension of the filament

ρ (kg/m^3) is the density of the filament

η (Pas) is the viscosity of the filament

Although the applicability of equation (30) to predict the growth of the capillary waves may be limited, it contains parameters which have been observed to affect surface instability and capillary break-up. Ziabicki [1, pp. 18-19] has modeled (by modifying equation (30)) the effect of varying surface tension and viscosity on the maximum draw length. These models predict that the break-up distance will increase with viscosity and decrease with surface tension, although at some point this behavior is asymptotic.

Ziabicki reports that capillary break-up has been observed in melt spinning of metals, inorganic glasses and polycondensates (polyamides, polyesters etc.) and in dry-spinning of polymer solutions. Ide and White [2] mention only low molecular weight LDPE (described as polymer wax) to break-up by capillarity. Thus it seems that Ide and White do not consider capillary break-up exist in practical fiber spinning. Ziabicki [1] mentions capillary break-up to be an important problem in melt dspinning of metals and Ide and White [2] mention ductile failure to occur in metal processing. These observations suggest that ductile failure introduced by Ide and White [2] and capillary break-up by Ziabicki describe the same phenomenon in practice at least to some extent.

5.2.4 Draw resonance and other instabilities

Steady oscillation of filament diameter leading to spinning instability has been widely observed in melt spinning but also in dry-jet wet spinning as was mentioned earlier. Petrie and Denn [37] as well as Larson [38] have reviewed the topic of draw resonance (as well as other instabilities occurring in fiber spinning). Recent studies are often fully theoretical and utilize computer modeling: *e.g.* German [39] *et al.* have investigated draw resonance and the following filament rupture (without aforementioned classification of the break-up method) on Newtonian liquids utilizing gravity and inertia on the mathematical model and Aarts *et al.* [40] modeled draw resonance as deflections perpendicular to the spin line. Examples of experimental studies of the topic can be found both in melt spinning *e.g.* Nam and Bogue [41], Han and Kim [42], Blyler and Gieniewski [43] and in dry-jet wet spinning *e.g.* Serkov and Afanas'eva [44]. There seems to be consensus that draw resonance is dependent on the extrusion velocity and draw-ratio. Han mentions that with a constant extrusion rate draw resonance will occur at some critical value of draw-ratio. [11, p. 315] If the draw-ratio is further increased, it can also lead to a failure of the spun filaments. White and Ide [2] consider draw resonance to be a continuous thread line analogue of ductile failure. Larson [38] considers non-stable oscillation which can lead to filament break-up as 'necking'. White and Ide [32] also mention that HDPE and PP tend to neck and exhibit ductile failure. Thus combining these observations one could suggest that ductile failure and failure by necking would describe the same phenomenon.

Ziabicki introduces also other instabilities which may occur in fiber spinning: 1. die swell, 2. irregular extrusion (melt fracture, observed in melt spinning) and formation of non-uniform fibers due to several reasons such as variation in processing conditions (varying take-up speed etc.). [1]

5.2.5 Structure of the spinnable liquid affecting spinnability

All authors who have reviewed the field of fiber spinning mention that viscosity and viscoelasticity are important properties affecting spinnability of polymer solutions and melts. Also surface tension in relation to viscoelasticity seems to be critical with some melts and solutions. Authors [1, 2, 3] have presented theoretically and empirically derived relations between rheological (at least elongational viscosity and relaxation time characteristics) and hydro dynamical (surface tension) parameters and spinnability in terms of maximum draw length and elongation.

White and Ide [2] have also related average molecular weight of polymer melts to maximum elongation of the spinning fluid. Their suggestion is that spinning with intermediate molecular weight melts fails by ductility and with high molecular weights the failure is cohesive. In the cohesive fracture range the spinnability should decrease with increasing molecular weight and in the ductile range spinnability should increase with increasing molecular weight. Ziabicki [1] reports the break-up mechanism to be dependent on the relation between surface tension and viscosity α/η. Decreasing surface tension and increasing viscosity, respectively, increase the probability of cohesive failure.

Michels and Kosan [16] mention that the stability of fiber spinning from NMMO is improved by increasing the ratio of high molecular weight cellulose chains in the spinning solution. Also increasing the mass fraction of low molecular weight chains has been noticed to decrease spinnability. However, theoretical analyses similar to those presented above were not found in dry-jet wet spinning and for Lyocell dry-jet wet spinning even experimental spinnability analysis of this kind was not found (spinnability related to the fiber structure such as orientation). Authors [16] also mention inhomogenities and size of particles in the spinning solution as one source of instable spinning.

Experimental:

6 Blend preparation & molecular weight distribution characterization

Part of the experimental objective was to prepare cotton linter (CL) blends with constant average molecular weight (M_w) while varying the molecular weight distribution (MWD). This approach was chosen in order to minimize the effect of varying average molecular weight and the varying amount of impurities (such as lignin) on the differences with the spinnability of cellulose-EMIMOAc solutions. In order to accomplish this task, cotton linters pulps with different M_w and intrinsic viscosity values were mixed in different weight ratios while targeting the intrinsic viscosity values of the blends on the same level. Intrinsic viscosity correlates with average molecular weight and it is easy to measure thus this method was chosen for fixing the M_w. MWD-properties were characterized by gel permeation chromatography (GPC).

6.1 Blend preparation

CLs which were utilized in the spinning solutions (dopes) were characterized by intrinsic viscosity according to SCAN-CM 15:99-standard and molecular weight distribution (MWD) by gel permeation chromatography (GPC) at Lenzing AG [45]. As blend components Milouban cotton linters (CL) 2, 3 and Kier-Boil degraded [46, 47] cotton linters 2 were utilized. Degraded cotton linters were utilized in the blends in order to enable low enough viscosity levels for the spinning dopes. Kier Boiling was utilized since the shape of the MWD of the degraded linters was expected to remain almost unchanged after the degradation with this method. Intrinsic viscosity and respective degree of polymerization (DP) values and GPC-data of the original pulps (components in blends) are presented in Table 1. DP-values are calculated from the intrinsic viscosity values [η] according to equation (31):

$$DP = \frac{[\eta]}{0.42} \quad when\ [\eta] \le 410\ \ (ml/g)$$
$$DP = \left(\frac{[\eta]}{2.28}\right)^{1/0.76} \quad when\ [\eta] > 410\ \ (ml/g) \tag{31}$$

Table 1. Values from the SCAN-CM 15:99 measurements and GPC-data.

Cotton linters	η (ml/g)	DP	Mn (kg/mol)	Mw (kg/mol)	Mz (kg/mol)	PDI	w (DP<50) (%)	w (DP<100) (%)	w (DP>2000) (%)
CL2	524	1280	119.8	216.2	356.3	1.805	0	0.5	17.9
CL3	909	2642	128.5	402.7	771.2	3.134	0.5	1.3	45
CL2 air-deg.1	255	607	38.8	82.2	137.4	2.120	2.8	7.3	1.2
CL2 air-deg.2	241	574	36.3	75.1	123.0	2.067	3.0	6.7	0.7

Five CL-pulp blends (Blend1, 2, 3, 4, 5) were prepared by mixing Milouban cotton linters (CL) 2, 3 and degraded cotton linters 2 (CL2 air-deg.1 and CL2 air-deg2) in different weight ratios while the intrinsic viscosity values of all the blends were targeted to be 450 ml/g. Thus the weight ratios of components in each blend were calculated according to the equation (32).

$$\sum_{i=1}^{N} w_i \cdot [\eta]_i = [\eta]_{target} \tag{32}$$

where

w_i is the weight fraction of the pulp i

$[\eta]_i$ (ml/g) is the intrinsic viscosity value of the pulp *i*

$[\eta]_{target}$ (ml/g) is the targeted intrinsic viscosity for the pulp blend

Blend compositions, predicted and measured intrinsic viscosity values are presented in Table 2. Blend5 was utilized only in a dope with 10 % cellulose concentration while others were utilized in 8 % dopes. 10 % dopes were problematic to prepare due to their high viscosity which made degassing of solutions problematic. Intrinsic viscosity of Blend5 was measured according to a DIN 54270 and respective SCAN-value was estimated based on the linear relation of the two standards. A curve showing the relation between the values of two standards is presented in Appendix A. Intrinsic viscosity values presented in Table 2 seem to suggest that an increase of the difference between the measured and predicted value with increasing proportion of CL3 in the blend. This could be followed by the higher degradation level of high molecular weight chains which CL3 contains more than the other two blend components.

Table 2. Compositions of Blend1-Blend5 and respective measured and predicted intrinsic viscosity values.

Blend	Cotton linters	weight ratio	$[\eta]_{measured}$ (ml/g)	$DP_{measured}$	$[\eta]_{predicted}$ (ml/g)
Blend1	CL2 air-deg.1	0.687	400	952	450
	CL3	0.313			
Blend2	CL2 air-deg.1	0.261	439	1014	450
	CL2	0.739			
Blend3	CL2 air-deg.1	0.399	441	1020	450
	CL2	0.500			
	CL3	0.101			
Blend4	CL2 air-deg.1	0.543	427	978	450
	CL2	0.250			
	CL3	0.207			
Blend5	CL2 air-deg.2	0.704	429	983	449
	CL3	0.296			

6.2 MWD-characteristics of blends

Utilizing GPC-data of the blend components, theoretical MWD data was calculated to all blends. This was accomplished by calculating the number of chains N_i^{blend} with molecular weight of M_i (g/mol):

$$N_i^{blend} = N_a \cdot m_{blend} \sum_k \left(\frac{w_i^k \cdot x^k}{M_i} \right) \tag{33}$$

where

N_a (1/mol) is the Avogadro number

m_{blend} (g) is the mass of the blend

w_i^k is the weight fraction of polymer chains having a molecular weight of M_i (g/mol) in the blend component k

x^k is the weight fraction of the component k in the blend

N_i can be utilized as a relative value in the average molecular weight calculations thus N_a and m_{blend} can be neglected from the equation (33).

The predicted and measured MWD values are presented in Table 3 for blends 1-4 (GPC-characterization was not executed for Blend5). Differences between the predicted and measured values do not seem to follow the same pattern as was noticed with intrinsic viscosity values. This could indicate that other physical phenomena than the polymer degradation affect the deviation from GPC-results to a higher extent. Possibly this deviation could follow from the inaccuracy of the GPC-measurement. Depending of the magnitude of the error of the GPC-method, it could be claimed that the predicted values give a good estimation of the measured values. MWD-graphs of the measured GPC-values of the blend components are presented in Figure 10 and respective data for the blends 1-4 is shown in Figure 11.

Table 3. Predicted and measured GPC-data of blends 1-4.

		Mn (kg/mol)	Mw (kg/mol)	Mz (kg/mol)	PDI	w (DP<50) (%)	w (DP<100) (%)	w (DP>2000) (%)
Blend1	predicted	47.0	177.8	582.8	3.780	2.2	5.3	14.4
	measured	49.3	187.5	610.3	3.803	2.1	4.9	15.2
Blend2	predicted	75.0	179.4	331.7	2.391	0.8	2.2	13.2
	measured	80.9	170	298.3	2.102	0.4	1.7	12.2
Blend3	predicted	62.9	178.9	412.3	2.842	1.3	3.2	13.6
	measured	63.5	174.6	410.3	2.748	1.2	3	13.3
Blend4	predicted	53.8	178.4	497.3	3.312	1.8	4.3	14.0
	measured	61.7	192.3	559.1	3.118	1.2	3.2	15.4

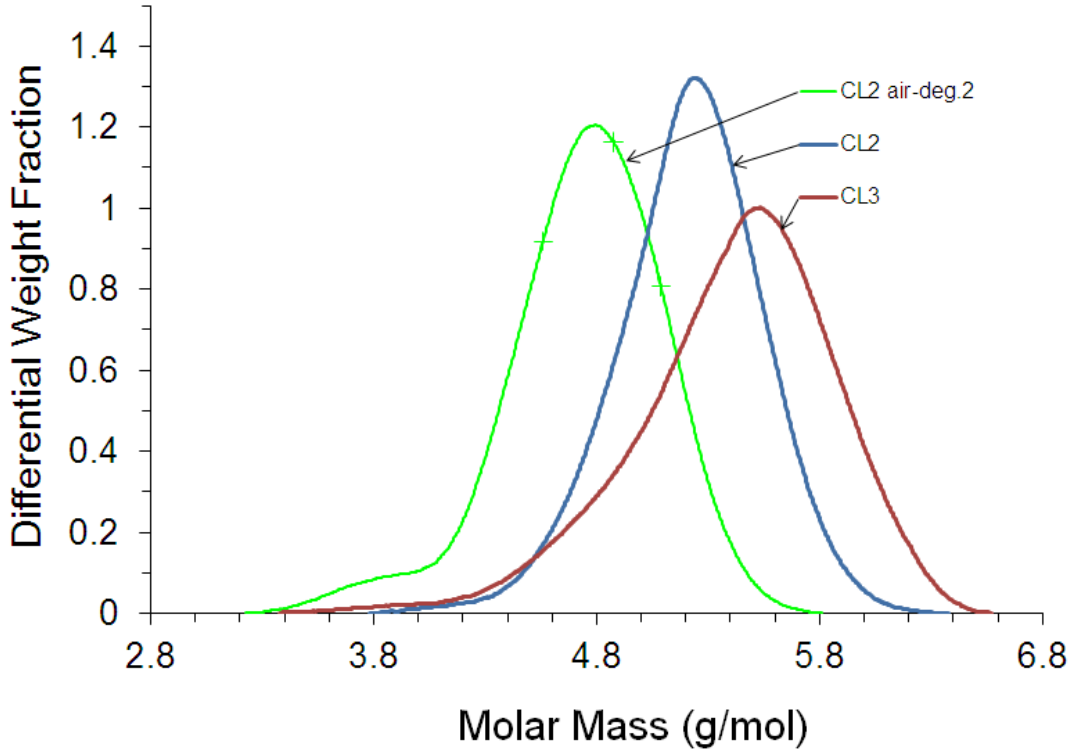

Figure 10. Logarithmic presentation of MWD-distribution of the components utilized with blends 1-4.

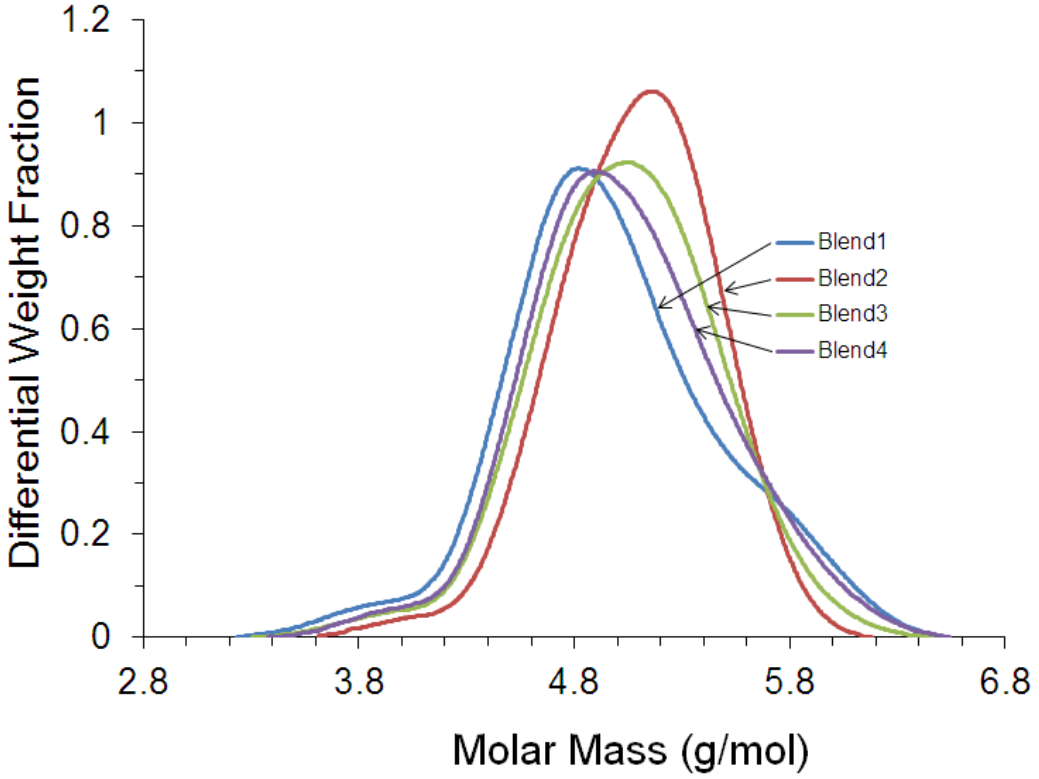

Figure 11. Logarithmic presentation of MWD-distribution of the blends 1-4.

7 Dope preparation & characterization by shear rheology

For the main research task four cellulose-EMIMOAc (1-ethyl-3-methylimidazolium acetate) solutions were prepared with 8 weight % cellulose concentration (referred as dope). This investigation was initially supposed to be accomplished with 10 wt % dopes but due to problems in the preparation phase lower concentration was utilized instead. Still, only one 10 wt % dope was spun successfully and thus observations from this dope are included here in order to evaluate the effect of concentration on spinnability.

7.1 Dope preparation

Four dopes (Dope1-Dope4) were prepared by mixing 8 wt % of blend with 92 wt % of EMIMOAc. Utilized EMIMOAc (manufactured by BASF) had a residual water content of 3.6 wt % and density of 1.027 g/l. All the dopes were prepared by mixing them in a rotational mixer with stirring rate of about 20 rpm at 20 °C for 30 min, at 20–80 °C for 30 min and at 80 °C for 1.5 h (overall 2.5 h). After the mixing, all the solutions were kept at 80 °C under a vacuum of about 200 mbar in order to degas the solutions. The degassing time varied a bit between the dopes since some of them required more time to be freed from air bubbles. Dopes are named Dope1, 2, 3, 4 and each dope contained blend with the corresponding number (*e.g.* Dope1 was prepared by mixing Blend1 with EMIMOAc). Dope5 was prepared in an analogous way to other dopes except the temperature evolution to 80 °C was not monitored as carefully and degassing time was considerably longer due to higher viscosity. The total heating-mixing phase was 166 min thus it could be estimated that it took about 0.5 h to raise the temperature to 80 °C. Details about the preparation of each dope are presented in Table 4. The most significant cellulose degradation during the preparation phase can be expected to happen at 80 °C in the mixing and degassing phase. Durations of these phases are thus reported.

Table 4. Dope compositions and preparation times.

Dope	Components	m (g)	$C_{cellulose}$ (%)	Mixing time at 80 °C (min)	Degassing time at 80 °C (h)
Dope1	Blend1	40.4	8	150	24
	EMIMOAc	464			
Dope2	Blend2	40.8	8	150	12
	EMIMOAc	469			
Dope3	Blend3	40.1	8	150	20
	EMIMOAc	462			
Dope4	Blend4	40.3	8	150	33
	EMIMOAc	463			
Dope5	Blend5	30.0	10	136	40
	EMIMOAc	270			

7.2 Rheological characterization

Rheological measurements for the spinning dopes have been performed with a Rheometrics DSR 500 rheometer with RSI Orchestrator-measuring program. All the measurements were executed with the same measuring setup with parallel plate geometry 25 mm measuring plate and 1 mm gap, a Peltier temperature control system and dynamic frequency sweep (FS) test measuring mode (stress control). Maximum stress was set to 400 Pa. Frequency sweep profiles were measured at 20, 40, 60, 80 and 100 °C from 100 Hz to 0.1 at 100 °C and from 100 to 1 Hz at other temperatures. Viscosity curves presented in Figure 12-Figure 14 have been fitted with Carreau model according to equation (34):

$$y = c_1(1+(c_2 x)^{c_3})^{(c_4-1)/c_3} \tag{34}$$

where

y (Pas) is the complex viscosity

x (rad/s) is the angular velocity

c_1-c_2 are fitting parameters

Dopes 1-4 were spun at a temperature range of 35-52 °C. Thus master curves derived from the measured frequency sweep data can be compared at the measurement temperatures from 40 to 60 °C. Master curve comparison at 40 °C is shown in Figure 12. Master curves of each dope in figures Figure 12-Figure 14 are derived from the whole measurement data of each dope. Viscosity data of each dope is fitted with the Carreau model (solid lines). Since the modulus curves are not fitted with a mathematical model but plotted as line graph instead, at higher shear rates some fluctuation is observed.

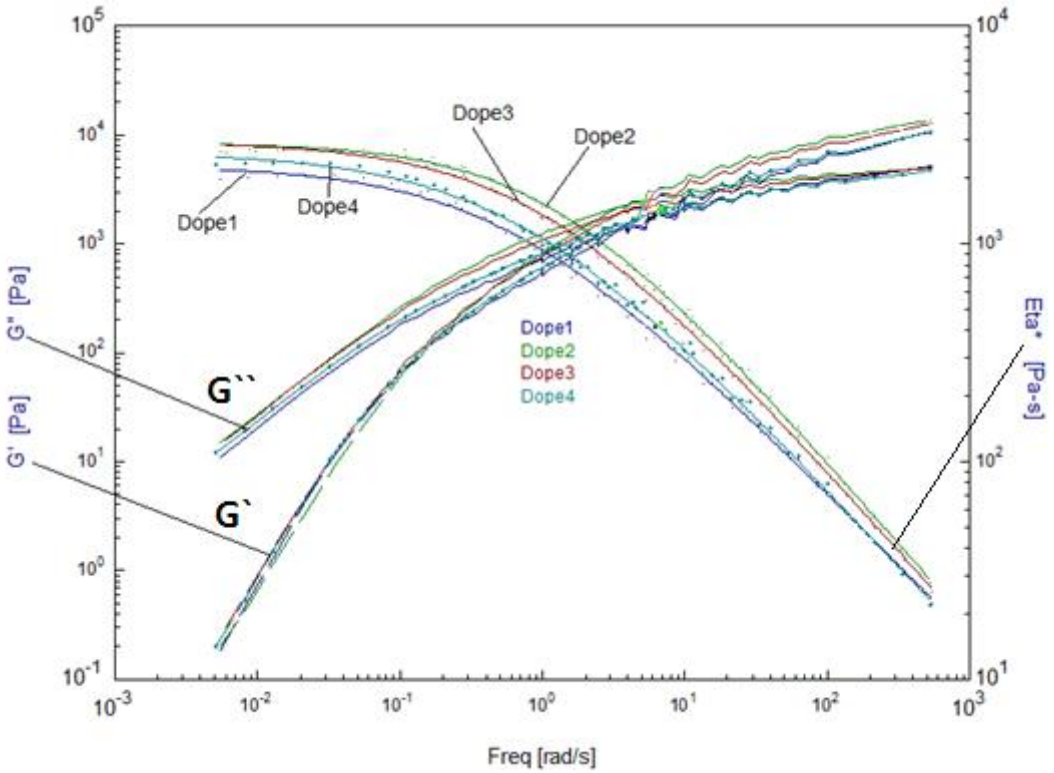

Figure 12. Frequency sweeps of dopes 1-4 at 40 °C. Storage moduli G` and loss moduli G`` are indicated by their symbols and viscosity by Eta. Colored name of each dope has the respective color as their curves.

The approach to the spinning trials included the target of similarity between the rheological states of each dope in the spinning process. This similarity in the process conditions was estimated based on the similarity of the FS-curves between different dopes. For this goal, the processing temperatures of each dope were chosen such their frequency sweep profiles between different dopes would superpose. Maximum temperature difference should be between Dope1 and 2 since they have the greatest differences with their FS-profiles. Thus the effect of temperature shift between 40-60 °C for Dope1 and 2 is shown in Figure 13.

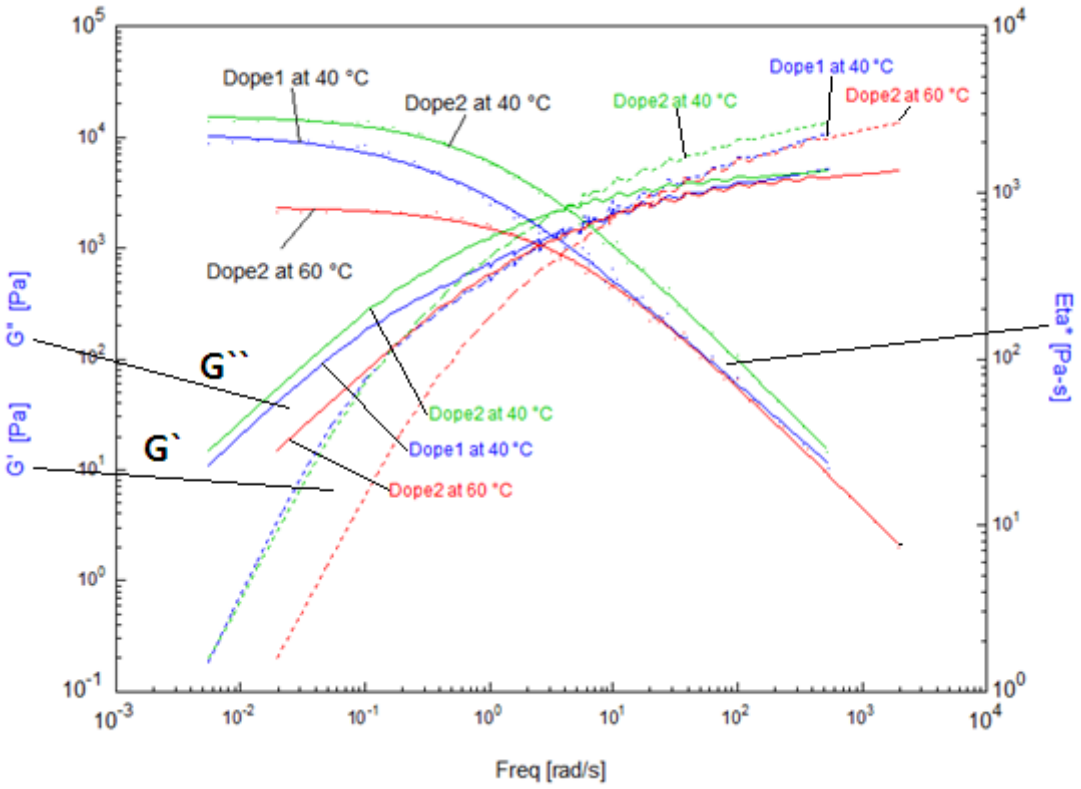

Figure 13. Comparison of frequency sweep profiles of Dope1 at 40 °C and Dope2 at 40 and 60 °C. It can be estimated that at high shear rates a temperature shift of about 10-20 °C leads to superposition of the dopes' curves.

It can be estimated that about 15-20 °C temperature difference in processing temperature for Dope1 and 2 makes their frequency sweep profiles almost equal at shear rates (frequencies) above 10 rad/s. For other dopes smaller temperature differences are required for the superposition. Similar comparison can be made between Dope1 and 5 which were predicted to have the most equal cellulose MWD properties of all the dopes. This superposition is shown in Figure 14.

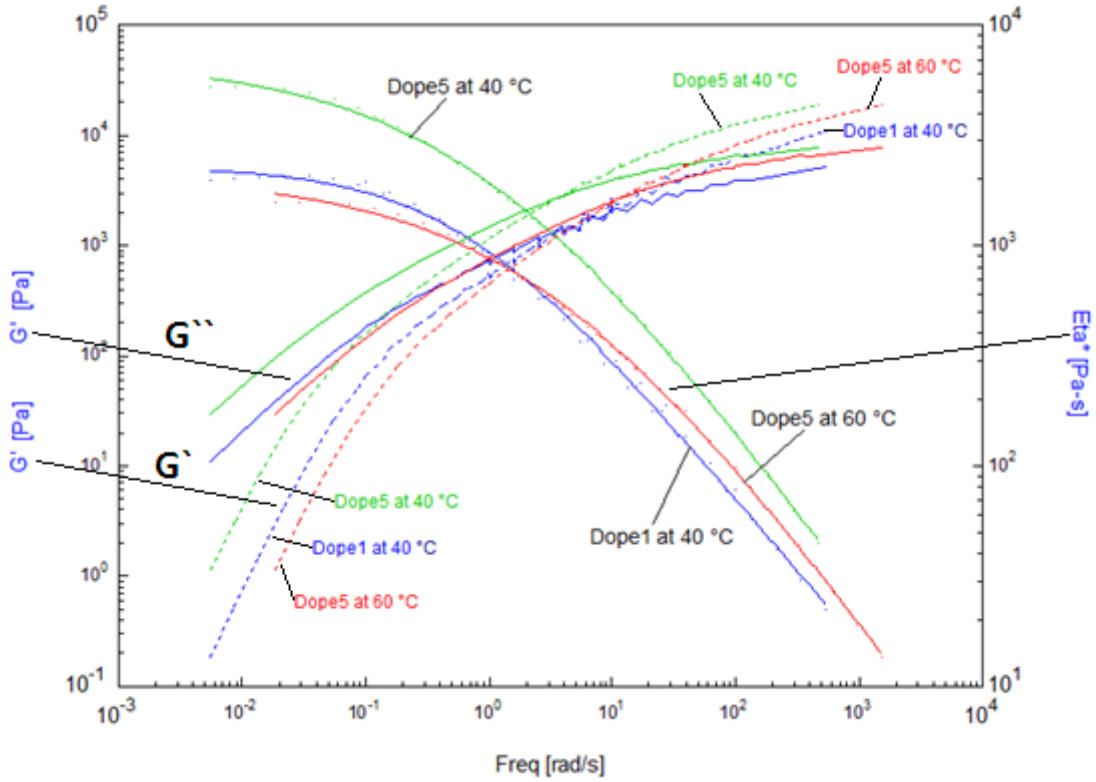

Figure 14. Comparison of frequency sweep profiles of Dope1 at 40 °C and Dope5 at 40 and 60 °C. It can be seen that a temperature shift of about 15-20 °C leads to an intersection of the dopes' curves. Complete superposition is not possible since FS-curves exhibit different shapes.

7.3 Relation between MWD and rheological parameters

Frequency sweep data of all the dopes were fitted with Carreau and Power law models (equation (1)). Parameters from these fits at different temperatures are shown in Table 5. With these parameter values the FS-curve of different dopes can be compared quantitatively. Parameter relations (shown in Table 5) between c_2 and c_1 from the Carreau-fit and between n and C from the Power law-fit are utilized in the following analysis instead of any single fit parameters. The idea of comparing these parameters is that the one utilized as the numerator relates more to the elastic behavior and the denominator to the overall viscosity of each dope (in other words: the numerator ↔ relaxation properties, denominator ↔ average viscosity and zero shear viscosity η_0).

Table 5. Parameters from the Power law and Carreau fits of FS-data from each dope.

Dope	Power law		Carreau				T (°C)	(10^4)*c_2/c_1	(10^3)*n/C
	C	n	$c_1 = \eta_0$	c_2	c_3	c_4			
Dope1	720	0.5239	2292	1.7302	0.6623	0.3315	40	7.55	0.73
	382	0.5003	623	0.4817	0.6694	0.3325	60	7.73	1.31
Dope2	1070	0.5129	2914	0.8446	0.7395	0.244	40	2.90	0.48
	604	0.4833	825	0.247	0.7473	0.2452	60	3.00	0.80
Dope3	1012	0.5073	2943	1.0527	0.678	0.2582	40	3.58	0.50
	572	0.476	859	0.3198	0.6866	0.2604	60	3.72	0.83
Dope4	800	0.5092	2638	1.4007	0.6258	0.2847	40	5.31	0.64
	448	0.4828	767	0.4273	0.6365	0.2874	60	5.57	1.08
Dope5	1545	0.5120	6928	0.9958	0.4303	0.2037	40	1.44	0.33
	859	0.4984	2076	0.2917	0.4284	0.2018	60	1.41	0.58
	570	0.4801	811	0.114	0.4284	0.2018	80	1.40	0.84

Utilizing similar principle as above, viscosity share $\eta_{crossover}$ (relates to viscosity properties) and the inverse of the angular velocity τ (relates to relaxation times properties) at the crossover point are have been related in Table 6 (this relation corresponds to $1/G_{crossover}$ as is shown below. Other parameters in shown in Table 6 are:

$\omega_{crossover}$ (rad/s) is the angular velocity at the crossover point

$G_{crossover} = G'' = G'$ (Pa) is the moduli level at the crossover point

$\eta_{crossover} = G_{crossover} / \omega_{crossover}$ (Pas) is the viscosity share at the crossover point

$\tau = 1/\omega_{crossover}$ (s) is the inverse of the angular velocity at the crossover point. This parameter should be related to relaxation properties of the solution.

$\tau/\eta_{crossover} = 1/G_{crossover}$ (Pa^{-1}) is a parameter relating relaxation and viscosity properties

Table 6. Rheological parameters from the crossover point characteristics from the FS-curves of each dope.

Dope	T (°C)	$\omega_{crossover}$ (rad/s)	$G_{crossover}$ (Pa)	$\eta_{crossover}$ (Pas)	100*τ (s)	$(10^5)*(\tau/\eta_{crossover})$ (Pa^{-1})
Dope1	40	6.2	1638.4	263.6	16.09	61.0
	60	22.5	1735.4	77.2	4.45	57.6
Dope2	40	3.7	2156.9	580.3	26.91	46.4
	60	13.5	2252.0	166.3	7.38	44.4
Dope3	40	3.6	1849.7	514.5	27.82	54.1
	60	12.7	1927.4	151.5	7.86	51.9
Dope4	40	4.2	1518.7	362.5	23.87	65.8
	60	14.8	1602.1	108.0	6.74	62.4
Dope5	40	3.5	2670.3	759.7	28.45	37.4
	60	12.8	2785.3	218.4	7.84	35.9
	80	34.1	2842.1	83.3	2.93	35.2

Parameter relations in Table 5 will be utilized in evaluation of the spinning results. At this point it can be noted that the n/C and c_2/c_1 at constant temperature (40 °C) values have the same order of magnitude as the PDI and M_z values between dopes 1-4. From all the fit parameters these two also seem to have the greatest differences between each dope which alone suggest relating them to MWD properties (along with the aforementioned relation between viscosity and relaxation properties). These parameters are highlighted in Table 7. Since M_n seem to have the greatest influence on viscosity and M_z on relaxation properties, these two could be also related to describe polydispersity which dominates the form of FS-curves. Parameter relations and τ in Table 6 do not follow the same pattern with Dope1 and 4 as the ones in Table 5, thus they are not utilized with the later analysis.

Table 7. GPC data and parameters n/C and c_2/c_1 (at 40 °C) for dopes 1-4.

Dope	Mn (kg/mol)	Mw (kg/mol)	Mz (kg/mol)	PDI	w (DP<50) (%)	w (DP<100) (%)	w (DP>2000) (%)	$10^4*c_2/c_1$ (at 40 °C)	$10^3*n/C$ (at 40 °C)
Dope1	49.3	187.5	610.3	3.803	2.1	4.9	15.2	7.55	0.73
Dope4	61.7	192.3	559.1	3.118	1.2	3.2	15.4	5.31	0.64
Dope3	63.5	174.6	410.3	2.748	1.2	3	13.3	3.58	0.50
Dope2	80.9	170	298.3	2.102	0.4	1.7	12.2	2.90	0.48

With Dope5 only the n/C values increase with temperature while c_2/c_1 do vice versa (as can be seen from Table 5). No GPC run was executed for Blend5 (corresponding to Dope5) and thus it is not included in the comparison above. However, the predicted PDI for Dope5 was 3.618 and even though the measured values may deviate from the predicted once significantly, this value can be expected to be in the range of 3.1-3.8 (Dope1 and 4). Thus it can be stated that either n/C or c_2/c1 values (at

constant temperature) of Dope5 do not follow the same order of magnitude with PDI values as with dopes1-4. Thus the higher cellulose concentration dominates parameters values over the PDI values for Dope5.

However, it might be more suitable to compare rheological parameters at temperatures where the viscosity properties (for example C-values) of each dope would be equal to each other. This would exclude the effect of temperature dependence of the parameters from the comparison. With this kind of temperature fixation also Dope5 might have the highest n/C values from all the dopes (lowering the viscosity level of Dope 5 requires increasing temperature which causes n/C values to increase). Utilized measurement program could not shift master curves to temperatures other than the ones utilized for the measurements thus the aforementioned method would be problematic to execute.

8 Spinning trials

The objective of the spinning trials was to examine differences in the maximum stretch ratio between dopes with similar FS-profiles at the processing temperatures. This approach was chosen to minimize especially the differences in viscosity between different dopes during the spinning process. Although the objective would suggest that only temperature and take-up velocity should be varied in the spinning trials, in practice extrusion velocity had to be varied in order to accomplish any spinning at all. Two main reasons that led to this necessity can be separated: 1. In practice it is problematic to control the solution characteristics and processing conditions in a way that it would allow to fulfill afore mentioned objective. 2. Even theoretically the rheological behavior of dopes processed at different temperatures would be different in the air gap (Filament temperature was discussed in the chapter 4.3).

8.1 Materials and methods

A Fourné lab scale piston spinning device was utilized for the spinning trials. A picture of the spinning equipment is presented in Figure 15. The coagulation bath was filled with tap water. Coagulation bath and air gap temperature were not controlled thus they can be evaluated to be approximately 20 °C. Positioning of the guide rollers and take-up wheel are presented in Figure 16.

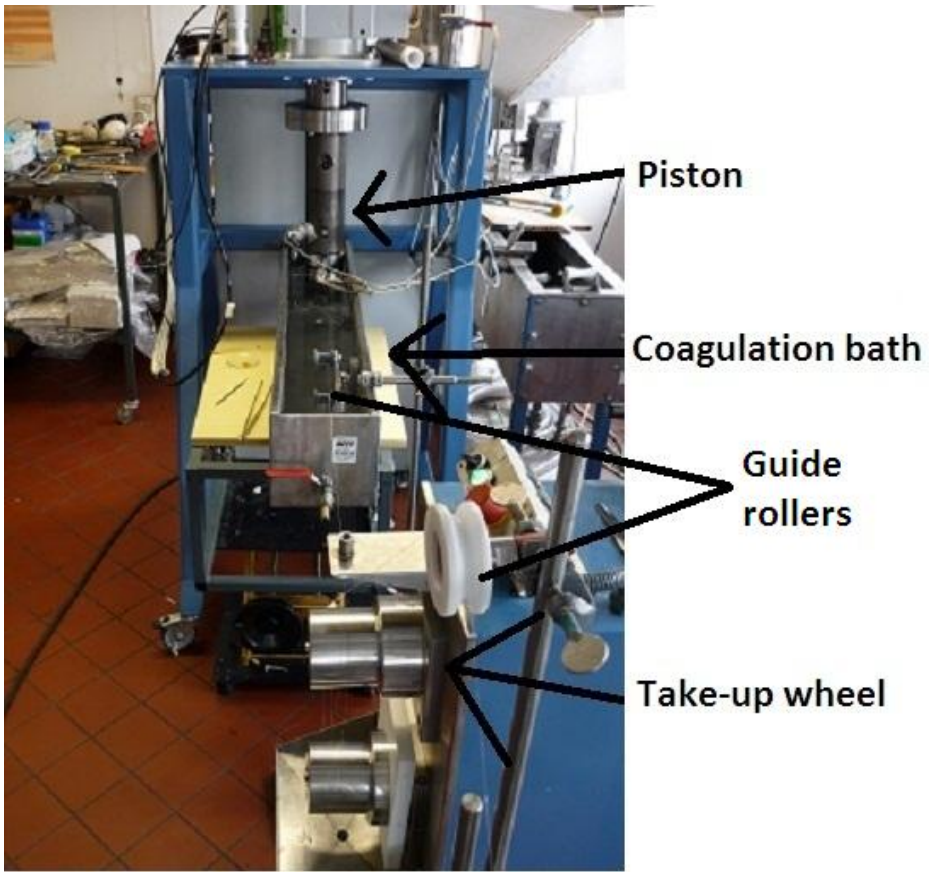

Figure 15. Picture of the spinning equipment.

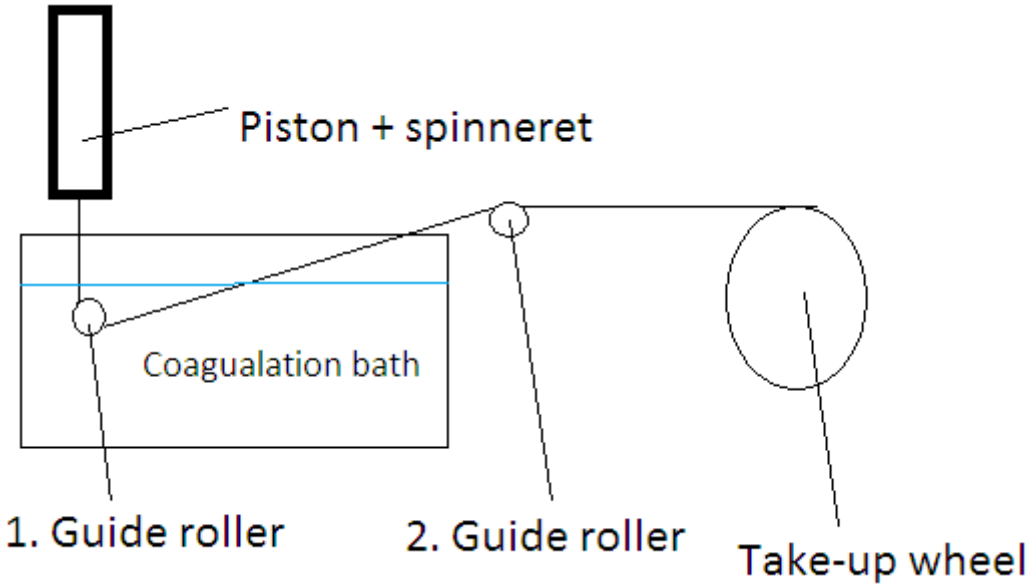

Figure 16. Schematic side view of the spinning equipment.

The geometry of the spinneret used in the spinning trials can be seen from the Figure 17 and Figure 18. The spinneret had 48 holes with nozzle length of 0.72 mm and diameter of 0.09 mm.

Figure 17. Alignment of the spinneret holes from the inlet side of the spinneret on left and from the extrusion side on right. The extrusion holes are placed in a same order as the inlet holes. Only the diameters of the extrusion holes are smaller than those of the inlet holes.

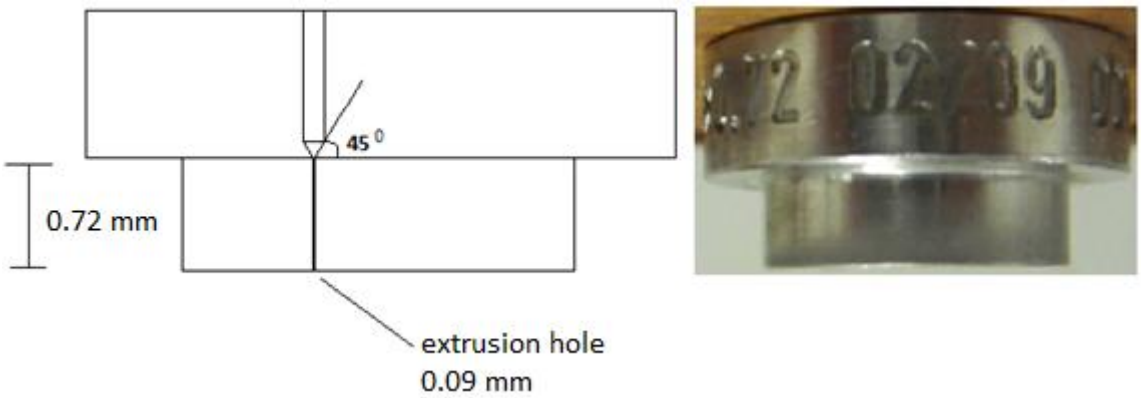

Figure 18. A schematic and real picture of the spinneret from the side view.

With dopes 1-4 the spinning trials were performed at the temperature range of 35–55 °C and extrusion volume velocities of 1.09-5.69 cm^3/min. Maximum stretch ratios were defined for fixed temperature-extrusion velocity combinations increasing the take-up and stretch ratio till filament break-up was observed. The purpose of trying different temperatures and extrusion velocities was to ensure that the differences in spinnability (maximum stretch ratio) of different dopes would follow from the solution characteristics and not from the verifying of the optimal spinning conditions of each dope. Thus the statistical certainty following from the amount of data was supposed to compensate the lack of understanding between the optimal processing conditions and dope characteristics. Dope5 (10 % dope) was not spun as systematically as the 8 % dopes. Maximum stretch ratios for Dope5 were determined only at two temperature-extrusion velocity combinations. Air gap length was adjusted to 4 cm in every trial.

8.2 Results and conclusions

8.2.1 Evaluation of results

Dopes 1-4 were spun in the order: Dope2, Dope1, Dope3 and Dope4. During the spinning trials, instead of systematic filament break-up with increasing stretch ratio random filament break-up was observed (break-up did not seem to be related to the position of the spinneret holes or the stretch ratio). It was also observed that even all but one filament broke the one remaining could be still stretched considerably. In order to decrease the effect of random filament break-up phenomenon on the determined spinnability limits, observed stretch limits were related to the number of rigid filaments. Different stretch limits that were observed during the trials are: 1 limit where no filament cuts are observed 2 limit where less than 50 % of the filaments are cut (more than 50 % are running), 3 limit where more than 50 % of the filaments are cut (less than 50 % are running), 4 limit where all the filaments are cut. The aforementioned spinnability limits are indicated in the result tables (Appendix B and Table 9) with different colors and brief comments in the comments cells. These colors and comments are explained in Table 8.

Only the limits 1 and 4 can be verified with good certainty (visibly confirm that either all the filaments are running or are cut). Due to the random effects mentioned above and the inaccuracy in adjusting the take-up velocity, there can be considerable

differences between different types of limits. In an ideal case 2 and 3 limit would be almost identical. For a monofilament only 1 and 4 type of limits could be observed. However, even then there would be a clear gap between the limits since determining the stable spinning limit 1 close to the break-up limit would require high accuracy from the processing and measuring equipment. Also referring to instabilities such as draw resonance, it can be argued that the stability of spinning is lost before the actual break-up.

Table 8. Indication colors and explanations for the number of cut filaments in the comments-column for different jet stretch limits. Comments in the brackets are utilized with the results shown in Appendix B together with individual notification of each limit.

jet stretch ratio limit	comments
1. limit	(0 cuts)
2. limit	(< 0.5 fil.)
3. limit	(> 0.5 fil.)
4. limit	(all fil. cut)

All the spinnability limits recorded in different processing conditions for Dope1, 3 and 4 are reported in Appendix B. Some of the results in Appendix B are described briefly to notify random effects occurring in the process. For the spinnability comparison only processing parameters and respective spinnability limits of type 1 and 2 are presented in Table 9. Dope5 was spun with a different experimental setting in mind thus only two limits were recorded for this dope. Spinning of Dope2 was problematic since the solution container started to leak from the hole of the pressure meter. For this reason it is fair to assume that the theoretically calculated extrusion velocities and stretch ratios are not realistic. However, the only obtained limit for Dope2 is included with other results.

Table 9. Highest jet stretch ratio limits of Dope1-5. For Dope1, 3, 4 three 2. limits are shown plus also one 1. limit for Dope1. For Dope2 and 5 no more limits were recorded.

Dope	T (°C)	V_{ram} (cm³/min)	$V_{extrusion}$ (m/min)	$V_{take-up}$ (m/min)	jet stretch ratio (%)	result number
Dope5	71.9	1.77	5.80	18.8	225	1.
	51.8	1.08	3.54	8.9	152	2.
Dope1	45.5	1.75	5.73	11.5	101	3.
	45.5	1.75	5.73	11	92	4.
	35.3	1.75	5.29	9.8	85	5.
	35.9	1.39	4.55	8.3	82	6.
Dope4	44.3	1.76	5.76	10	74	7.
	44.5	1.4	4.58	7.8	70	8.
	44.2	1.4	4.58	7.8	70	9.
Dope3	50.8	2.31	7.56	10.9	44	10.
	47.6	1.36	4.45	6.4	44	11.
	40.9	1.75	5.73	7.8	36	12.
Dope2	55.1	5.69	17.19	21.00	22	13.

In order to estimate the rheological states of the dopes in the spinneret, equations (7) and (8) were utilized to calculate shear rates, viscosities and stresses occurring with the utilized spinning parameters. However, even when the power law index n was set as one, the resulting viscosity levels were lower than the viscosity level of pure EMIMOAc (no cellulose added). Thus power law does not seem applicable to model spinneret flow for the chosen experimental setting. Qualitatively it can be assumed that the shear rates and stresses are high in the spinneret.

Analyzing the spinning results from dopes 1-4 was supposed to show the effect of MWD on the spinnability. However, due to aforementioned technical problems Dope2 is excluded from this analysis. It can be seen that the dopes 1, 3 and 4 follow the order: Dope1, Dope4, Dope3 with decreasing spinnability limit magnitude. Because this order is the same with different parameter combinations (as can also be verified from the Appendix B), it is unlikely that small differences in processing conditions between each dope would explain this phenomenon. As was stated previously, Dope1 and 4 had similar frequency sweep profiles at the same temperature. Comparison with results 3-4 from Dope1 and result 7 from Dope4 should be justified also because of the similar processing parameters. As was shown previously, Dope1 and 2 could be superposed by a temperature shift of 10-20 °C. Dope3 being similar to Dope2 should superpose with Dope1 and 4 with the same temperature shift. Thus comparing result 5 from Dope1 to results 10 and 11 from Dope3 could be justified with the superposition approach.

8.2.2 The effect of cellulose MWD and concentration on spinnability

Spinnability rankings based on the previously presented results of dopes 1, 3, and 4 are compared to GPC-data of the blends of each dope in Table 10. It can be seen that the ranking is improving with increasing PDI and M_z. At least between Dope1 and 4, PDI shows more correlation with the improvement of spinnability ranking. However, both

figures indicate that the fraction of high molecular weight cellulose affects spinnability the most.

Table 10. Stretch limits and measured GPC-data of dopes 1, 3 and 4. Parameters which seem to be correlating are marked with green color.

Dope	spinnability ranking	Mn (kg/mol)	Mw (kg/mol)	Mz (kg/mol)	PDI	w (DP<50) (%)	w (DP<100) (%)	w (DP>2000) (%)
Dope1	1.	49.3	187.5	610.3	3.803	2.1	4.9	15.2
Dope4	2.	61.7	192.3	559.1	3.118	1.2	3.2	15.4
Dope3	3.	63.5	174.6	410.3	2.748	1.2	3	13.3

Polydispersity values can be expected to show a relation with rheological parameters relating average viscosity and relaxation properties of a spinning solution. Thus the previously mentioned parameter relations from Carreau and Power law-fit could be related to PDI and M_z of dopes when the average molecular weights and solute concentrations of the compared dopes are close enough to each other. As it was discussed in the rheological characterization chapter, these parameter relations seem to have the greatest differences of all the single parameters between each dope. Curve fit parameters, PDI, M_z and spinnability rankings are shown in Table 11.

Table 11. Spinnability rankings, M_z, PDI and curve fit parameters c_2/c_1 c_2/η_0, n/C.

Dope	spinnability ranking	Mz (kg/mol)	PDI	10^4*c_2/η_0 (at 40 °C)	10^3*n/C (at 40 °C)
Dope1	1.	610.3	3.803	7.55	0.73
Dope4	2.	559.1	3.118	5.31	0.64
Dope3	3.	410.3	2.748	3.58	0.50
Dope2	4.	298.3	2.102	2.90	0.48

Dope5 with 10 % cellulose concentration seemed to have significantly better spinnability than any of the 8 % dopes. As was discussed in chapter 7, parameter relations did not anymore follow the same patter as they did with 8 % dopes. Thus the improved spinnability with increased concentration is not indicated with an increase of the aforementioned rheological parameters (which seemed to apply for 8 % dopes). As it was mentioned in the chapter 7.3, it would be interesting the utilize n/C-values with a fixed C-value for the comparison presented previously. Also utilizing n/C-values determined at the processing temperatures of different dopes for the spinnability comparison would be interesting.

8.2.3 Fiber MWD and mechanical properties

Fibers from the spinning trials of Dope1, 3 and 4 were characterized by GPC to evaluate cellulose degradation in the whole processing chain. In order to gain an overview of the fiber properties, fineness, elongation and tenacity were determined from the fiber samples of each blend/dope. These samples were collected from a random set of fibers spun with different processing parameters. Thus these results might describe any values between the minimum and maximum value of the fiber samples presenting each dope. MWD-data of the blends and respective fibers from dopes 1, 3 and 4 are shown in Table 12.

Table 12. GPC-data of blends 1, 3 and 4 and fibers processed of these.

		Mn (kg/mol)	Mw (kg/mol)	Mz (kg/mol)	PDI	w (DP<50) (%)	w (DP<100) (%)	w (DP>2000) (%)
Blend1	cotton linters	49.3	187.5	610.3	3.803	2.1	4.9	15.2
	fiber	71	152.5	308.8	2.149	0.4	2	10
Blend3	cotton linters	63.5	174.6	410.3	2.748	1.2	3	13.3
	fiber	53.1	156.6	419.6	2.949	1.4	4	12.3
Blend4	cotton linters	61.7	192.3	559.1	3.118	1.2	3.2	15.4
	fiber	61.9	166.3	415.9	2.685	0.9	3	12.7

Based on the results in Table 12, the order of magnitude of PDI values has changed which if considered as an undeniable fact, would turn many previous conclusions about the effect of MWD on spinnability vice versa. If the PDI values measured from fibers would characterize the cellulose MWD in the solution in the spinning process, spinnability would seem to improve with M_n.

To show why the MWD-values of the fibers do not seem realistic to be describing the solution structure the evaluation in chapter 7.2 and Figure 12 should be revised. The difference between the average viscosity of Dope4 and Dope3 (Blend4 and 3) is considerable and was estimated to require 10-20 °C temperature difference to equalize them. Based on the data measured from fibers, this difference would follow from the slight difference with the M_z-values of these two blends. If M_z would have this kind of effect, then Dope1 could be considered to have considerably lower viscosity than the other two dopes. Since the rheological characterization was executed right before the spinning trials, it is highly unlikely that significant cellulose degradation with the MWD-characteristics would occur between this and the processing phase.

Changes with the MWD of Blend1 and 3 seem to have developed in opposite directions. To visualize this, MWD of Blend1 and 3 and respective fibers are presented in Figure 19. The same presentation for Blend1 and 4 is presented depicted in Figure 20.

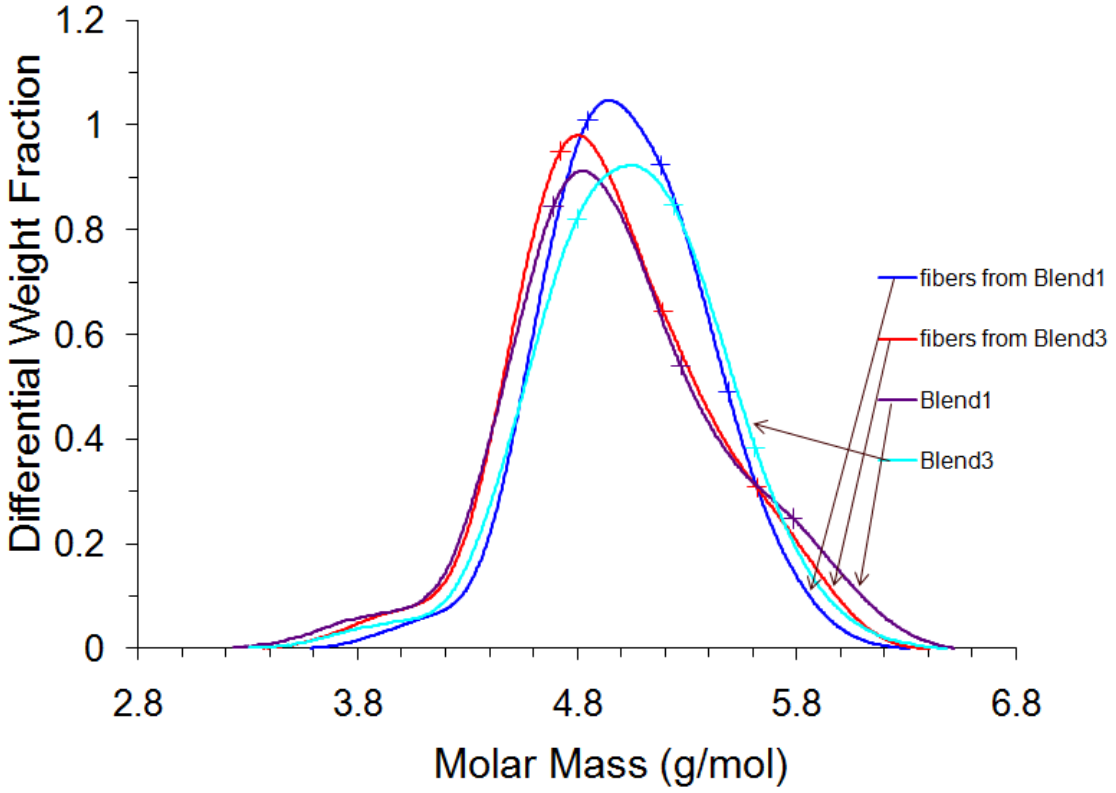

Figure 19. Logarithmic presentation of MWD-distribution of blends 1, 3 and the respective fibers.

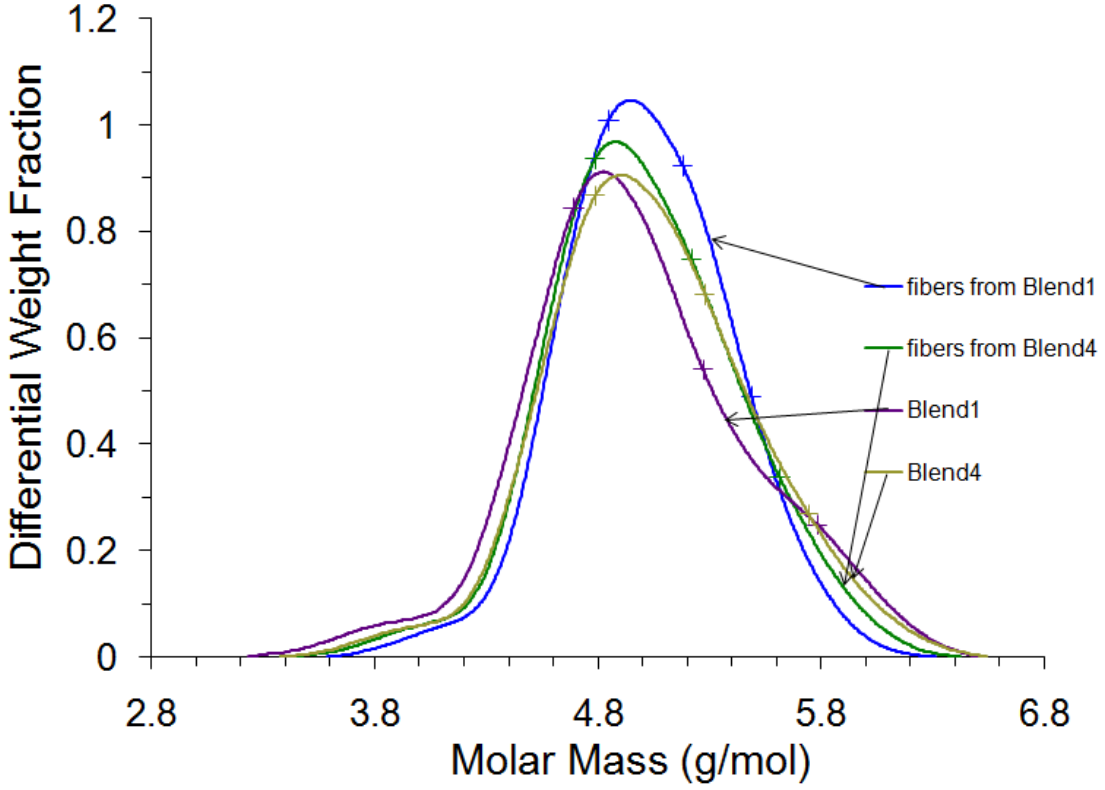

Figure 20. Logarithmic presentation of MWD-distribution of blends 1, 3 and the respective fibers.

In order to evaluate the physical nature of these results, an assumption of ideal measurement where GPC could measure all the separate molecules is utilized. The increase of average molecular weight values like M_n for Blend1 should not be theoretically possible unless chains with lower weight than the original average weight would disappear or chains with higher than the average value would be added. Based on the Figure 19 lower weight chains would have disappeared from Blend1 and some higher weight chains would have been added to Blend3 between the change of cotton linters to fibers. If MWD changes of Blend1 would be realistic, the lack of similar changes to Blend4 would be problematic to explain. The increase in the number of lower molar mass chains (in the region of 4.6-5.6 log(Molar Mass) resulting from the degradation of higher molar mass chains (from 5.8-6.6 log(Molar Mass)) with Blend1 seems logical. Same phenomenon is visible also with Blend4 within the same and for Blend3 within lower molar mass ranges.

Before analyzing physical phenomena related to aforementioned MWD changes, utilization of GPC for this purpose should be reviewed carefully. This issue was already mentioned in chapter 6 when the sources of differences between predicted and measured GPC results were mentioned.

Dry and wet values of fineness/titer, elongation and tenacity data from fibers spun from dopes 1, 3, and 4 are presented in Table 13. As was stated before, a random sample of fibers derived from different dopes were chosen for the measurements. The aforementioned properties were determined from five fiber samples of each thread sample. For this reason any results cannot be related to specific processing conditions. As can be seen, these results have a high deviation following from the aforementioned random selection of the samples.

Table 13. Titer, elongation and tenacity of dry and jet fibers. Minimum titer values of all the fiber samples have been marked with blue and maximum elongation and tenacity with red color.

		dry			wet		
		Titer (dtex)	**Elongation (%)**	**Tenacity (cN/tex)**	**Titer (dtex)**	**Elongation (%)**	**Tenacity (cN/tex)**
Dope1	average	22.86	10.14	13.44	29.4	22.48	7.46
	min	16.68	3.2	7.45	11.13	11.8	2.79
	max	38.98	13.5	15.93	53.85	32.5	10.13
Dope2	average	21.49	10.14	13.44	24.8	23.4	4.74
	min	16.77	10.2	13.81	19.3	1.9	0
	max	27.39	18.2	16.98	28.88	43.6	7.36
Dope3	average	14.4	11.98	18.33	10.82	10.58	6.97
	min	10.72	9.2	17.01	6.95	1.1	0.01
	max	18.88	15.2	19.35	18.65	15.7	10.06
Dope4	average	13.22	13.2	15.28	10.97	22.5	8.3
	min	10.29	8.2	11.47	9.21	13	6.93
	max	18.97	22.8	17.97	13.69	29.3	9.25

8.3 Discussion

Han [3] suggest that increasing relaxation times improves elastic strength while increasing viscosity increases the probability of cohesive fracture. Thus the relation of relaxation times/viscosity could limit spinnability in terms of rheological properties. This assumption would support the approach of examining the relation of viscosity and relaxation properties with spinnability. With a fixed concentration and average molecular weight (to some accuracy) curve fit parameters showed the same trend as the spinnability limits. Once the concentration was increased this trend was not anymore observed. However, it was noted that the compared rheological parameters should be measured from the processing temperatures. This method would have given considerably higher n/C values for the Dope5 which had a higher cellulose concentration than the other dopes.

Based on the results it can be qualitatively stated that the increase of fraction (increased with polydispersity) and the total amount (increased with concentration) of high molecular weight cellulose polymers increase the spinnability of cellulose-EMIMOAc solution. The aforementioned relation between viscosity and relaxation times could also set the limit for the number of high weight polymer chains in a solution [3].

Even a simple model which would combine viscosity and relaxation time(s) would help to evolve the explanation of limited spinnability. This could offer understanding of the aforementioned trend with spinnability and rheological parameters and the effect of high molecular weight chains on spinnability. In practice other issues might limit spinnability. For example for a cellulose-EMIMOAc solution degradation of cellulose at high temperatures and other practical problems (such as the quality of dissolution) in solution preparation would limit the applicable solution viscosity and thus the number of high molecular weight chains.

As it was stated before, it is problematic to prepare dopes with highly equal rheological properties. On the other hand, dopes with different rheological properties have different optimal processing conditions. In the experimental of this work, the main concern was about the differences with the viscosity of different dopes. This problem was approached by utilizing the processing temperature differences between the dopes in a way that their FS-curves (master curves) would superpose. However, in the processing situation there were also differences in the pressure and extrusion velocity values. Based on the reviewed literature, extrusion velocity affects the air-gap rheology. Pressure is known to affect viscosity, but it affects only in extrusion part. Also the temperature level should affect the air-gap rheology. Thus the utilization of the superposing principle can be questioned if it can be stated that the spinning rheology between different dopes varies greatly despite the temperature adjustment. Recognizing the importance of these spinning parameters would help to implement future spinnability investigations. Luckily, the comparison between the spinnabilities of different dopes was also based on the results from almost equal processing conditions. This decreases the risk of wrong conclusions following from an inadequate understanding of the theory.

9 Summary

As it was already stated in the chapter 8.3, the spinnability of cellulose-EMIMOAc seems to be improved with increasing PDI of cellulose when the average molecular weight and concentration of cellulose are fixed to some accuracy. To improve the exactness of the experimental and analysis of results in this type of spinnability investigation, theoretical understanding of the physical phenomenon occurring in spinning process should be elaborated further. This concerns at least two fields which were discussed in the literature part of this thesis: 1. The structure formation in dry-jet-wet spinning 2. Filament break-up and instability in spinning process. Naturally, these fields are paired to a large extent.

The main challenges of the first field are the determination of elongational viscosity, deformation rate and stress. Especially the separation of the effects of temperature change and elongational deformation rate on elongational viscosity would be essential. In a practical spinning process viscosity of a filament seems to increase with the distance from the spinneret and thus with the deformation rate. The measurements of elongational viscosity with *e.g.* capillary break-up rheometry have shown the viscosity to decrease with increasing deformation rate (which is analogous to shear viscosity measurements).

The importance of the second field is evident when the filament break-up is related to spinnability. Even though there is no consensus of the break-up mechanism classification, it seems that viscosity and relaxation time properties are always affecting the break-up while surface tension is considered when it is high enough compared to the other two. These properties might relate to break-up limits via maximum filament tension and elongation rate. Recognizing the key rheological parameters and their relation to break-up should improve the whole investigation chain starting from the rheological characterization.

As well as the theoretical field, also the utilized experimental execution could be elaborated on. One previously mentioned idea was about the rheological characterization and the rheological parameters utilized for comparisons between different dopes. It was suggested that either viscosity parameter C would be fixed or measured from the spinning temperatures when n/C-values would be utilized for the comparison between different dopes. Developing the aforementioned issues should improve spinnability investigations generally and not solely for a cellulose-EMIMOAc system.

References

[1] A. Ziabicki. *Fundamentals of Fibre Formation- The Science of Fibre Spinning and Drawing.* New York, John Wiley & Sons, 1976. ISBN 0471982202.

[2] Y. Ide, J. L. White. The spinnability of polymer fluid filaments. *Journal of Applied Polymer Science*, 1976, Vol. 20, No. 9, pp. 2511-2531.

[3] C. D. Han. A Theoretical Study on Fiber Spinnability. *Rheologica Acta*, 1970, Vol. 9, No. 3, pp. 355-365.

[4] S. A. Mortimer, A. A. Péguy. The Formation of Structure in the spinning and coagualtion of Lyocell Fibres. *Cellulose Chemistry and Technology*, 1996, Vol 30, pp 117-132.

[5] S. A. Mortimer, A. A. Péguy, R. C. Ball. Influence of the Physical Parameters on the Structure Formation of Lyocell Fibres. *Cellulose Chemistry and Technology*, 1996, Vol 30, pp. 251-266.

[6] S. A. Mortimer, A. A. Péguy. The Influence of Air-Gap Conditions on the Structure Formation of Lyocell Fibers. *Journal of Applied Polymer Science*, 1996, Vol. 60, No. 10, pp. 1747-1756.

[7] T. G. Mezger. *The Rheology Handbook*. 2nd Edition. Hannover, Vincent Network GmbH & Co., 2006 ISBN 3-87870-174-8.

[8] L. A. Shelley, G. H. McKinley. Elasto-capillary thinning and breakup of model elastic liquids. *Journal of Rheology*, 2005, Vol. 45, No. 1, pp. 115-138.

[9] W. Ostwald. Ueber die rechnerische Darstellung des Strukturgebietes der Viskosität. *Colloid and Polymer Scince*. 1929,Vol. 47, No. 2, pp. 176-187.

[10] H. P. Fink, P. Weigel, H.J. Purz, J. Ganster. Structure formation of regenerated cellulose materials from NMMMO solutions. *Prog. Polym. Sci*, 2001 No. 26, pp. 1473-1524

[11] C. D. Han. *Rheology in Polymer Processing*. London, Academic Press, 1976. ISBN 0-12-322450-0.

[12] J. F. Agassant, P. Avenas, J. P. Sergent, P. J. Carreau. *Polymer Processing – Principles and Modeling.* 2. Edition. Munich. Hanser. ISBN 3-446-14584-2.

[13] P. Weigel, H. P. Fink, E. Walenta, J. Ganster, H. Remde. Structure Formation of Cellulose Man-Made Fibres from Amine Oxide Solution. *Cellulose Chemistry Technology*, 1997, Vol 31, pp. 321-333.

[14] F. Wendler, B. Kosan, M. Krieg, F. Meister.. Possibilities for the physical modification of Cellulose Shapes Using Ionic Liquids. *Macromol. Symp*., 2009, Vol. 280, No. 1, pp. 112-122.

[15] B. Kosan, C. Michel, F. Meister. Dissolution and forming of cellulose with ionic liquids. *Cellulose*, 2008, No. 15, pp. 59-66.

[16] C. Michels, B. Kosan. Lyocell process – material and technological restrictions. *Chemical Fibers International*, 2000, Vol. 50, pp. 556-561.

[17] J. R. Collier, O. Romanoschi, S. Petrovan. Elongational Rheology of Polymer Melts and Solutions. *Journal of Applied Polymer Sciences*, 1998, Vol 69, pp. 2357-2367.

[18] L. L. Chapoy. A Phenomenological description of viscoelastic memory in capillary flow. *Rheologica Acta*, 1969, Vol. 8, pp. 497-503.

[19] J. L. White, J. F. Roman. Extrudate Swell During the Melt spinning of Fibers-Influence of Rheological Properties and Take-up force. *Journal of Applied Polymer Science*, 1976, Vol. 21, No. 4, pp. 1005-1023.

[20] Y. Ide, J. L. White. Instabilities and Failure in Elongational Flow and Melt Spinning of Fibers. *Journal of Applied Polymer Science*, 1978, Vol. 22, No. 11, pp. 3057-3074.

[21] R. Liu, H. Shao, X. Hu, C. Wu, X. Hu. An Analysis of Lyocell Fiber Formation as a Melt-spinning Process. *Cellulose*, 2001, Vol. 8, pp. 179.186.

[22] P. Navard, J. M. Haudin, I. Quenin, A. Péguy. Shear rheology of diluted solutions of high molecular weight cellulose. *Journal of Applied Polymer Science*, 1986, Vol. 32, No, 7, pp. 5829-3839.

[23] M.M. Denn, C. J. S. Petrie, P. Avenas. Mechanics of steady spinning of a viscoelastic liquid. *AIChE Journal*, 1975, Vol. 21, No. 4, pp. 791-799.

[24] P. Navard, J. M. Haudin. The Spinning of Cellulose methylmorpholine oxide Solution. *Polymer Processing Engineering*, 1996, Vol. 60, pp. 1747-1756.

[25] S. A. Mortimer, A. A. Péguy. A Device for On-Line Measurement of Fiber Birefringence. *Textile Research Journal*, 1994, Vol. 64, Issue 9, pp. 544-551.

[26] D. R. Paul. A study of spinnability in the wet-spinning of acrylic fibers. *Journal of Applied Polymer Science*, 1968, Vol. 12, pp. 2273-2293.

[27] L. Tan, H. Chen, D. Pan, N. Pan. Investigating the Spinnabilty in the Dry-jet Wet Spinning of PAN Precursor Fiber. *Journal of Applied Polymer Science*, 2008, Vol. 110, No. 4, pp. 1997-2000.

[28] K. Hashimoto, T. Imae. The Spinnability of Aqueous Polymer Solutions. *Polymer Journal*, 1990, Vol. 22, No. 4, pp. 331-335.

[29] Y. Ide, J. L. White. Investigation of Failure during Elongational Flow of Polymer Melts. *Journal of Non-Newtonian Fluid Mechanics*, 1977, Vol. 2, No. 3, pp. 281-298.

[30] O. Hassager, M. I. Kolte, M. Renardy. Failure and Nonfailure of Fluid Filaments in Extension. *Journal of Non-Newtonian Fluid Mechanics*. 1998, Vol. 76, No. 1-3, pp. 137-151.

[31] H. Tabuteau, S. Mora, G. Porte, M, Abkarian, C. Ligoure. Microscopic Mechanism of the Brittleness of Viscoelastic Fluids. *Physical Review Letters*, 2009, Vol. 102, No. 15, p. 4.

[32] Y. Ide, J. L. White. Experimental study of elongational flow and failure of polymer melts. *Journal of Applied Polymer Science*, 1978, Vol. 22, No. 4, pp. 1061-1071.

[33] A. Y. Malkin, C. J. S. Petrie. Some conditions for rupture of polymer liquids in extension. *Journal of Rheology*, 1997, Vol. 41, No. 1, pp. 1-25.

[34] Y. Wang, P. Boukany, S. Wang, X, Wang. Elastic Breakup in Uniaxial Extension of Entangled Polymer Melts. *Physical Review Letters*, 2007, Vol. 99, No. 23, p. 4.

[35] J. Eggers. Non-linear dynamics and break-up of free-surface flows. *Reviews of Modern Physics*, 1997, Vol. 69, No. 3, pp. 865-929.

[36] C. Weber. Zum Zerfall eines Flüssigkeitsstrahles. *Zeitschrift für Angewandte Mathematik und Mechanik*, 1931, Vol. 11, No. 2, pp. 136-154.

[37] C. J. S. Petrie, M. M. Denn. Instabilities in polymer processing. *AIChE Journal*, 1976, Vol. 22, No. 2, pp. 209–236.

[38] R. G. Larson. Instabilities in Viscoelastic Flows. *Rheologica Acta*, 1992, Vol. 31, No. 3, pp. 213-263.

[39] R. German, R. E. Khayat, J. K. Cui. Influence of Inertia and Gravity on the Stability of Filament Jet Flow. *Physics of Fluids*, 2006, Vol. 18, No. 6, 16 pages.

[40] A. C. T. Aarts, S. J. L. van Eijndhoven, O. Zavinska. Traveling Waves along Viscous Filaments. *Journal of Engineering Mathematics*, online publication, 2011, pp. 1-18. Cited 22.6.2011. DOI 10.1007/s10665-011-9466-4.

[41] S. Nam, D. C. Bogue. Dynamics of Steady and Unsteady Melt Spinning. *Industrial & Engineering Chemistry Fundamentals*, 1984, Vol. 23, No. 1, pp. 1-8.

[42] C. D. Han, Y. W. Kim. Studies on Melt Spinning. VI. The Effect of Deformation History on Elongational Viscosity, Spinnability, and Thread Instability. *Journal of Applied Polymer Science*, 1976, Vol. 20, pp. 1555-1571.

[43] L. L. Blyler, G. Gieniewski. Melt spinning and draw resonance studies on a poly (α-methyl styrene/silicone) block copolymer. *Polymer Engineering Science*, 1980, Vol. 20, Issue 2, pp. 140-148.

[44] A. T. Serkov, Y. V. Afanas'eva. Flow of Solution through Spinneret Openings and Deformation Resonance. *Fibre Chemistry*, 1999, Vol. 31, No. 3, pp. 192-196.

[45] N. Schelosky, T. Röder. T. Baldinger. Molmassenvertailung cellulosischer Produkte mittels Größenausschlußchromatographie in DMAc/LiCl. *Das Papier*, 1999, Vol 12, pp. 728-738.

[46] N. Nazir, M. U. Parmar, K. Venkataraman. Chemical processing of Indian cotton linter materials. I The effect of kier boiling and bleaching on the cuprammonium fluidity and strength of yarns spun from four good-quality Indian cottons. *Journal of the Indian Chemical Society, Industrial and News Edition*, 1941, Vol 4, No. 2, pp. 93-110.

[47] N. Nazir, M. U. Parmar, K. Venkataraman. Chemical processing of Indian cotton linter materials. II Influence of different concentrations of caustic soda on the quality of kier-boiled and bleached yarns spun from Indian cottons. *Journal of the Indian Chemical Society, Industrial and News Edition*, 1946, Vol. 9, pp. 1-21.

Appendix A: Comparison between DIN 54270 (DP-values) and Scan-CM 15:99 intrinsic viscosity values

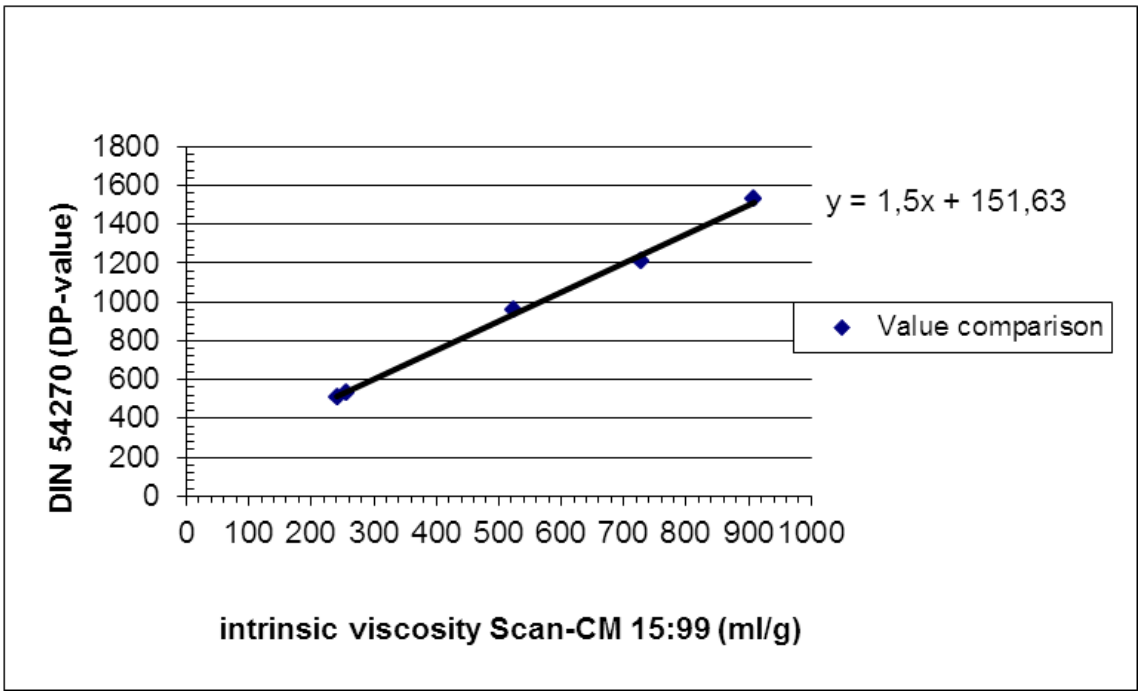

Appendix B: Recorded spinnability limits for Dope1, 3 and 4

Table B1. Spinning trial results for Dope1.

Run	h_{air} (cm)	P (bar)	T (°C)	V_{ram} (cm³/min)	$V_{extrusion}$ (m/min)	$V_{take-up}$ (m/min)	jet stretch ratio (%)	comments
1	4	72.3	35.3	1.75	5.73	9.8	71	Ok fibers (< 0.5 fil.)
	4	72.3	35.3	1.75	5.73	10.9	90	many filaments cut (> 0.5 fil.)
2	4	64	35.9	1.39	4.55	8.3	82	Ok fibers few cuts (< 0.5 fil.)
	4	64	35.9	1.39	4.55	9	98	many filaments cut (> 0.5 fil.)
3	4	85.3	35.8	2	6.55	9.8	50	Ok fibers few cuts (< 0.5 fil.)
	4	85.3	35.8	2	6.55	10.3	57	many filaments cut (> 0.5 fil.)
4	4	50.9	45.5	1.75	5.73	11	92	Ok fibers (0 visible cuts)
	4	50.9	45.5	1.75	5.73	11.5	101	Ok fibers few cuts (< 0.5 fil.)
	4	50.9	45.5	1.75	5.73	12.4	116	(all fil. cut)
	4	52.4	44.7	1.75	5.73	10.6	85	Ok fibers (0 visible cuts)
5	4	64.3	42.2	1.99	6.52	12.1	86	filaments start to cut slowly (> 0.5 fil.) and form non-uniformities
	4	49.2	43.8	1.39	4.55	8.1	78	Ok fibers few cuts (< 0.5 fil.)

Table B2. Spinning trial results for Dope3.

Run	h_{air} (cm)	P (bar)	T (°C)	V_{ram} (cm³/min)	$V_{extrusion}$ (m/min)	$V_{take-up}$ (m/min)	jet stretch ratio (%)	comments
1	4	52.4	40.9	1.75	5.73	7.8	36	Ok fibers few cuts (< 0.5 fil.)
2	4	not recorded	51.8	1.75	5.73	7.8	36	many filaments cut (> 0.5 fil.)
3	4	48.1	50.8	2.31	7.56	10.9	44	Ok fibers few cuts (< 0.5 fil.)
	4	51.6	49.2	2.31	7.56	11.4	51	many filaments cut (> 0.5 fil.)
	4	53	49.2	2.31	7.56	10.6	40	Ok fibers few cuts (< 0.5 fil.) verification of the previous limit
4	4	not recorded	49	2.61	8.55	11	29	Ok fibers few cuts (< 0.5 fil.)
	4	not recorded	49	2.61	8.55	12.4	45	(all fil. cut)
5	4	38.6	47.6	1.36	4.45	6.4	44	Ok fibers, 0 cutting at first but after a while some random cutting (< 0.5 fil.)
	4	39.6	47	1.36	4.45	6.3	41	Ok fibers, some random cutting verification of the previous limit (< 0.5 fil.)

Table B3. Spinning trial results for Dope4.

Run	h_{air} (cm)	P (bar)	T (°C)	V_{ram} (cm^3/min)	$V_{extrusion}$ (m/min)	$V_{take-up}$ (m/min)	jet stretch ratio (%)	comments
1	4	42	44.2	1.4	4.58	7.8	70	Ok fibers few cuts (< 0.5 fil.)
	4	42	44.2	1.4	4.58	8.4	83	many filaments cut (< 0.5 fil.)
	4	42.7	44.7	1.4	4.58	8.6	88	(all fil. cut)
	4	43.5	44.5	1.4	4.58	7.8	70	Ok fibers few cuts (< 0.5 fil.) verification of the previous limit
2	4	53	44.1	1.75	5.73	9	57	Ok fibers few cuts (< 0.5 fil.)
	4	54.1	43.9	1.75	5.73	9.5	66	many filaments cut (< 0.5 fil.)
3	4	43.8	42.2	1.09	3.57	6	68	Ok fibers few cuts (< 0.5 fil.) but close to > 0.5 fil.cut
	4	43.8	42.2	1.09	3.57	6.7	88	many filaments cut (< 0.5 fil.)
4	4	49.8	44.3	1.76	5.76	10	74	Ok fibers few cuts (< 0.5 fil.)
	4	49.8	44.3	1.76	5.76	10.2	77	0.1- 0.5 filaments cut, form non-uniformities
	4	49.8	44.3	1.76	5.76	11.6	101	many filaments cut (> 0.5 fil) form non-uniformities
	4	49.8	44.3	1.76	5.76	12.2	112	(all fil. cut)
5	4	48.3	47	1.76	5.76	8.8	53	Ok fibers (0 cutting at first but after a while some random cutting)
	4	48.3	47	1.76	5.76	10.2	77	many filaments cut (> 0.5 fil)
6	4	48.4	51.8	2.02	6.62	10	51	Ok fibers few cuts (< 0.5 fil.)
	4	48.4	51.8	2.02	6.62	11.5	74	many filaments cut (> 0.5 fil.)
	4	48.4	51.8	2.02	6.62	12.3	86	(all fil. cut)
7	4	48.4	42.8	1.41	4.62	7.1	54	Ok fibers few cuts (< 0.5 fil.)
	4	48.4	42.8	1.41	4.62	8.7	88	many filaments cut (< 0.5 fil.)
	4	48.4	42.8	1.41	4.62	9.2	99	(all fil. cut)
	4	48.4	42.8	1.41	4.62	8.9	93	many filaments cut (> 0.5 fil.) verification of the previous limit
	4	48.4	42.8	1.41	4.62	9.6	108	(all fil. cut)